Effects of neutral Z' boson in $B_s \to \varphi\ell^+\ell^-$ decay with polarized φ and the unpolarized and polarized CP violation asymmetry

Ishtiaq Ahmed,[1,2,*] M. Jamil Aslam,[2,†] and M. Ali Paracha[3,4,‡]

[1]*National Centre for Physics, Quaid-i-Azam University Campus, Islamabad 45320, Pakistan*
[2]*Department of Physics, Quaid-i-Azam University, Islamabad 45320, Pakistan*
[3]*Centre for Advanced Mathematics and Physics, National University of Science and Technology,
Islamabad 44000, Pakistan*
[4]*Laboratorio de Física Teórica e Computacional, Universidade Cruzeiro do Sul,
São Paulo 01506-000, Brazil*

The effects of the new neutral Z' boson in $B_s \to \varphi\ell^+\ell^-$, when φ is longitudinal or transverse polarized, are studied. In addition, the implications of the Z' boson on the unpolarized and polarized CP violation asymmetries, with reference to leptons, are also presented. It is observed that the branching ratio with polarized φ is quite sensitive to the Z' contributions which are coming through the modification of the Wilson coefficients C_9^{eff} and C_{10}. Moreover, the off-diagonal elements of the chiral Z' couplings contain a new weak phase φ_{sb} that provides a new source of CP violation. Keeping in view that in the flavor-changing neutral-current transitions, the CP-violation asymmetries are highly suppressed in the Standard Model, we have studied the unpolarized and polarized CP-violation asymmetries in $B_s \to \varphi\ell^+\ell^-$ decays. Our results indicate that these CP-violation asymmetries are remarkably significant and can give us hints of any new physics coming through the Z' boson. It is hoped that accurate measurements of these asymmetries will not only help us to establish NP but also give us a chance to determine the precise values of the coupling parameters of the Z' boson.

I. INTRODUCTION

The purpose of high-energy experiments is to resolve the unanswered questions in the Standard Model (SM) through searches of new physics (NP) using complementary approaches. The first approach is at the energy frontier, where the key representatives are the ATLAS and CMS experiments at the Large Hadron Collider (LHC) at CERN. The main purpose of these two detectors is to smash particles at sufficiently high energy and then study the different particles produced after the collision. The second approach is at the rare/precision frontier, where the LHCb experiment at the LHC and the Belle II at the super-KEKB are two important experiments with regard to flavor physics.

In the precision approach, the observable signature of new particles or processes can be obtained through the measurement of flavor physics reactions at lower energies and the collection of evidence of any deviation from these predictions. A natural place to start is to investigate the flavor-changing neutral-current (FCNC) processes in B-meson decays, where one of the heavy quarks makes them an ideal laboratory to test the nonperturbative aspects

of the QCD and also makes them a fertile hunting ground for testing the SM and probing the possible NP effects.

Undoubtedly, the predictions of the SM are in good agreement with the collider data until now; however, there still exist some mysteries that are unanswered in this model. Just to name a few, they include neutrino oscillations, baryon asymmetry, dark matter, unification, the strong CP violation, and the hierarchy problems. To answer these issues, there exist a plethora of NP models such as the extra dimension models, various supersymmetric models, etc. In grand unification theories such as $SU(5)$ or string-inspired $E6$ models [1–5], some of the most pertinent are the Z' scenarios that include the family nonuniversal Z' [6,7] and leptophobic Z' models [8,9].

It is well known that the gauge group $SU(5)$ can be extended to the next important group $SO(10)$, which has one extra rank, and hence leads to an idea of an extra heavy neutral Z boson [10]. Even though Z' gauge couplings are family universal [11–15], due to different constructions of the different families in string models, it is possible to have family nonuniversal Z' couplings. For example, in some of them, three generations of leptons and also the first and second generations of quarks have different couplings to the Z' boson when compared to the third families of quarks [7,16,17]. The details about this model can be seen, for instance, in Refs. [6,18–23].

Searching for an extra Z' boson is an important mission of the Tevatron [24] and LHC [25] experiments. Performing

*ishtiaq@ncp.edu.pk
†jamil@phys.qau.edu.pk
‡ali@ncp.edu.pk

constraints on the new Z' couplings through low-energy precise processes is, on the other hand, very crucial and complementary for these direct searches of $Z' \to e^+e^-$ at the Tevatron [26]. It is interesting to note that such a family nonuniversal Z' model could bring new CP-violating phases beyond the SM and have a large effect on many FCNC processes [27,28], such as the $B_s - \bar{B}_s$ mixing [29–33], as well as some rare [34] and hadronic B-meson decays [35,36].

In the present study, we will analyze the $B_s \to \varphi \ell^+ \ell^-$ decay in the family nonuniversal Z' scenario. At quark level, this decay is governed by the FCNC transition $b \to s\ell^+\ell^-$, which arises at loop level in the SM because of the Glashow-Ilipoulos-Maiani mechanism, where the new heavily predicted particles of different models can manifest themselves. In particular, by analyzing the different physical observables like the decay rate, the forward-backward asymmetry, and different lepton polarization asymmetries and comparing them with the SM predictions, one can test the SM as well as find the traces of the physics beyond it. A detailed analysis of the above mentioned physical observables in the family nonuniversal Z' model for $B_s \to \varphi \ell^+ \ell^-$ is discussed at length in Ref. [37]. However, the study of the polarized and unpolarized CP-violation asymmetries as well as the polarized branching ratio is still missing in the literature.

With the motivation that the behavior of the other observables in the presence of the Z' boson may play a crucial role in redefining our knowledge about the family non-universal Z' model, we have studied both polarized and unpolarized CP-violation asymmetries and the polarized branching ratio for $B_s \to \varphi \ell^+ \ell^-$ in the SM and the Z' model. In the context of CP-violation asymmetry, it is important to emphasize that the FCNC transitions are proportional to three Cabibbo-Kobayashi-Maskawa (CKM) matrix elements, namely $V_{tb}V_{ts}^*$, $V_{cb}V_{cs}^*$, and $V_{ub}V_{us}^*$; however, due to the unitarity condition, and neglecting $V_{ub}V_{us}^*$ in the comparison of $V_{tb}V_{ts}^*$ and $V_{cb}V_{cs}^*$, the CP-violation asymmetry is highly suppressed in the SM. Therefore, the measurement of CP-violation asymmetries in FCNC decays plays a pivotal role in finding the signatures of the Z' model.

This paper is schemed as follows: In Sec. II, we briefly describe the theoretical formulation necessary for the transition $b \to s$, including effective Hamiltonian matrix elements in terms of form factors, and then define the amplitude by using these matrix elements. In Sec. III, we give the explicit expression of the polarized branching ratio, as well as polarized and unpolarized CP-violation asymmetries for $B_s \to \varphi \ell^+ \ell^-$. Section IV presents the phenomenological analysis and discussion on the numerical results. The summary of the results and concluding remarks will also be given in the same section.

II. THE $B_s \to \varphi \ell^+ \ell^-$ TRANSITION IN THE SM AND FAMILY NONUNIVERSAL Z' MODEL

A. The SM effective Hamiltonian

The effective Hamiltonian for the decay channel $B_s \to \varphi \ell^+ \ell^-$ with $\ell = \mu, \tau$, proceeding through the quark level transition $b \to s\ell^+\ell^-$ in the SM, can be written as

$$H_{\text{eff}} = -\frac{4G_F}{\sqrt{2}} V_{tb}^* V_{ts} \sum_{i=1}^{10} C_i(\mu) O_i(\mu), \quad (1)$$

where G_F is a Fermi coupling constant and V_{ij} are the matrix elements of the CKM matrix. In Eq. (1), $O_i(\mu)$ $(i = 1, \ldots, 10)$ are the four-quark operators and $C_i(\mu)$ are the corresponding Wilson coefficients at the energy scale μ, and the explicit expressions of these Wilson coefficients at next-to-leading order and next-to-next-leading logarithm are given in Refs. [38–48]. By considering the fact that $\frac{V_{ub}V_{us}^*}{V_{tb}V_{ts}^*} < 0.02$, we have neglected the terms proportional to $V_{ub}V_{us}^*$. The operators responsible for $B_s \to \varphi \ell^+ \ell^-$ are O_7, O_9, and O_{10}, and their forms are given by

$$O_7 = \frac{e^2}{16\pi^2} m_b (\bar{s}\sigma_{\mu\nu}P_R b) F^{\mu\nu},$$

$$O_9 = \frac{e^2}{16\pi^2} (\bar{s}\gamma_\mu P_L b)(\bar{l}\gamma^\mu l),$$

$$O_{10} = \frac{e^2}{16\pi^2} (\bar{s}\gamma_\mu P_L b)(\bar{l}\gamma^\mu \gamma_5 l), \quad (2)$$

with $P_{L,R} = (1 \pm \gamma_5)/2$. Neglecting the strange quark mass, the effective Hamiltonian [Eq. (1)] gives the following matrix element:

$$\mathcal{M}(B_s \to \varphi \ell^+ \ell^-)$$
$$= \frac{\alpha_{\text{em}} G_F}{2\sqrt{2}\pi} V_{tb} V_{ts}^* \Big[\langle \varphi(k, \varepsilon) | \bar{s}\gamma^\mu (1 - \gamma^5) b | B_s(p) \rangle$$
$$\times \{ C_9^{\text{eff}} (\bar{l}\gamma_\mu l) + C_{10} (\bar{l}\gamma_\mu \gamma^5 l) \}$$
$$- 2C_7^{\text{eff}} m_b \langle \varphi(k, \varepsilon) | \bar{s} i\sigma_{\mu\nu} \frac{q^\nu}{s} (1 + \gamma^5) b | B_s(p) \rangle (\bar{l}\gamma^\mu l) \Big],$$
$$(3)$$

where α_{em} is the electromagnetic coupling constant calculated at the Z-boson mass scale. Also, $q = p_1 + p_2$ is the momentum transfer to the final lepton pair, where p_1 and p_2 are the momenta of ℓ^- and ℓ^+, respectively, and s is the square of the momentum transfer.

The Wilson coefficient $C_9^{\text{SM}}(\mu)$, with the commonly used notation $C_9^{\text{eff}}(\mu)$, corresponds to the semileptonic operator O_9. It can be decomposed into three parts:

$$C_9^{\text{SM}} = C_9^{\text{eff}}(\mu) = C_9(\mu) + Y_{\text{SD}}(z, s') + Y_{\text{LD}}(z, s'), \quad (4)$$

where the parameters z and s' are defined as $z = m_c/m_b$, $s' = q^2/m_b^2$. The function $Y_{\text{SD}}(z, s')$, corresponding to

short distance, describes the perturbative part, which includes the indirect contributions from the matrix element of four-quark operators $\sum_{i=1}^{6}\langle l^{+}l^{-}s|O_{i}|b\rangle$, and this lies sufficiently far away from the $c\bar{c}$ resonance regions. The manifest expressions for $Y_{\mathrm{SD}}(z,s')$ can be written as [49,50]

$$
\begin{aligned}
Y_{\mathrm{SD}}(z,s') = &\; h(z,s')(3C_{1}(\mu)+C_{2}(\mu)+3C_{3}(\mu) \\
&+ C_{4}(\mu)+3C_{5}(\mu)+C_{6}(\mu)) \\
&- \frac{1}{2}h(1,s')(4C_{3}(\mu)+4C_{4}(\mu)+3C_{5}(\mu)+C_{6}(\mu)) \\
&- \frac{1}{2}h(0,s')(C_{3}(\mu)+3C_{4}(\mu)) \\
&+ \frac{2}{9}(3C_{3}(\mu)+C_{4}(\mu)+3C_{5}(\mu)+C_{6}(\mu)),
\end{aligned}
\tag{5}
$$

with

$$
h(z,s') = -\frac{8}{9}\ln z + \frac{8}{27} + \frac{4}{9}x - \frac{2}{9}(2+x)|1-x|^{1/2}
$$
$$
\times
\begin{cases}
\ln\left|\dfrac{\sqrt{1-x}+1}{\sqrt{1-x}-1}\right| - i\pi & \text{for } x \equiv 4z^{2}/s' < 1 \\
2\arctan\dfrac{1}{\sqrt{x-1}} & \text{for } x \equiv 4z^{2}/s' > 1
\end{cases},
$$

$$
h(0,s') = \frac{8}{27} - \frac{8}{9}\ln\frac{m_{b}}{\mu} - \frac{4}{9}\ln s' + \frac{4}{9}i\pi.
\tag{6}
$$

The long-distance contributions $Y_{\mathrm{LD}}(z,s')$ from four-quark operators near the $c\bar{c}$ resonance cannot be calculated from first principles of QCD and are usually parameterized in the form of a phenomenological Breit-Wigner formula making use of the vacuum saturation approximation and quark-hadron duality. In the present study, we ignore this part because this lies far away from the region of interest.

The Wilson coefficient C_{7}^{eff} is given by [51–53]

$$
C_{7}^{\mathrm{SM}} = C_{7}^{\mathrm{eff}}(\mu) = C_{7}(\mu) + C_{b\to s\gamma}(\mu),
\tag{7}
$$

with

$$
C_{b\to s\gamma}(\mu) = i\alpha_{s}\left[\frac{2}{9}\eta^{14/23}(G_{1}(x_{t}) - 0.1687) - 0.03C_{2}(\mu)\right],
\tag{8}
$$

$$
G_{1}(x_{t}) = \frac{x_{t}(x_{t}^{2}-5x_{t}-2)}{8(x_{t}-1)^{3}} + \frac{3x_{t}^{2}\ln^{2}x_{t}}{4(x_{t}-1)^{4}},
\tag{9}
$$

where $\eta = \alpha_{s}(m_{W})/\alpha_{s}(\mu)$, $x_{t} = m_{t}^{2}/m_{W}^{2}$, $C_{b\to s\gamma}$ is the absorptive part for the $b\to sc\bar{c}\to s\gamma$ rescattering, and we have dropped out the tiny contributions proportional to CKM sector $V_{ub}V_{us}^{*}$.

B. The effective Hamiltonian in the Z' model

In the Z' model, the presence of off-diagonal couplings make the FCNC transitions occur at tree level. Ignoring the Z–Z' mixing and the interaction of right-handed quarks with Z', the new gauge boson contribution only modifies the Wilson coefficients C_{9} and C_{10} [54]. With these assumptions, the extra part that is added to the Hamiltonian given in Eq. (1) can be written as follows [55–57]:

$$
\begin{aligned}
\mathcal{H}_{\mathrm{eff}}^{Z'} = &-\frac{2G_{F}}{\sqrt{2}}\bar{s}\gamma^{\mu}(1-\gamma^{5})b\mathcal{B}_{sb}[\mathcal{S}_{\ell\ell}^{L}\bar{\ell}\gamma^{\mu}(1-\gamma^{5})\ell \\
&- \mathcal{S}_{\ell\ell}^{R}\bar{\ell}\gamma^{\mu}(1+\gamma^{5})\ell] + \mathrm{H.c.},
\end{aligned}
\tag{10}
$$

where $\mathcal{B}_{sb} = |\mathcal{B}_{sb}|e^{-i\varphi_{sb}}$ is the off-diagonal, left-handed coupling of the Z' boson with quarks, and φ_{sb} corresponds to a new weak phase. The left- and right-handed couplings of the Z' boson with leptons are represented by $\mathcal{S}_{\ell\ell}^{L}$ and $\mathcal{S}_{\ell\ell}^{R}$, respectively. Therefore, one can also write the above equation in the following way:

$$
\mathcal{H}_{\mathrm{eff}}^{Z'} = -\frac{4G_{F}}{\sqrt{2}}V_{tb}V_{ts}^{*}[\Lambda_{sb}C_{9}^{Z'}\mathcal{O}_{9} + \Lambda_{sb}C_{10}^{Z'}\mathcal{O}_{10}] + \mathrm{H.c.},
\tag{11}
$$

with

$$
\Lambda_{sb} = \frac{4\pi e^{-i\varphi_{sb}}}{\alpha_{s}V_{tb}V_{ts}^{*}},
\tag{12}
$$

$$
C_{9}^{Z'} = |\mathcal{B}_{sb}|S_{LL}; \qquad C_{10}^{Z'} = |\mathcal{B}_{sb}|D_{LL},
\tag{13}
$$

$$
S_{LL} = \mathcal{S}_{\ell\ell}^{L} + \mathcal{S}_{\ell\ell}^{R}; \qquad D_{LL} = \mathcal{S}_{\ell\ell}^{L} - \mathcal{S}_{\ell\ell}^{R}.
\tag{14}
$$

In short, to include the Z' effects in the problem under consideration, one has to make the following replacements to the Z-boson Wilson coefficients C_{9} and C_{10}, while C_{7} remains unchanged:

$$
C_{9}' = C_{9}^{\mathrm{eff}} + \Lambda_{sb}C_{9}^{Z'}, \qquad C_{10}' = C_{10} + \Lambda_{sb}C_{10}^{Z'}.
\tag{15}
$$

C. Matrix elements and form factors

The $B_{s} \to \varphi\ell^{+}\ell^{-}$ decay can be obtained by sandwiching the effective Hamiltonian between the initial-state B_{s} and the final-state φ meson. This can be parameterized in terms of the form factors as follows:

$$
\langle\varphi(k,\varepsilon)|\bar{s}\gamma_{\mu}b|B_{s}(p)\rangle = \varepsilon_{\mu\nu\rho\sigma}\varepsilon^{*\nu}p^{\rho}k^{\sigma}\frac{2V(q^{2})}{M_{B_{s}} + M_{\varphi}},
\tag{16}
$$

$\langle\varphi(k,\varepsilon)|\bar{s}\gamma_\mu\gamma_5 b|B_s(p)\rangle$

$$= i\varepsilon_\mu^*(M_{B_s} + M_\varphi)A_1(q^2) - i(p+k)_\mu(\varepsilon^* \cdot q)\frac{A_2(q^2)}{M_{B_s} + M_\varphi}$$

$$- iq_\mu(\varepsilon^* \cdot q)\frac{2M_\varphi}{q^2}[A_3(q^2) - A_0(q^2)], \qquad (17)$$

$$\langle\varphi(k,\varepsilon)|\bar{s}\sigma_{\mu\nu}q^\nu b|B_s(p)\rangle = i\varepsilon_{\mu\nu\rho\sigma}\varepsilon^{*\nu}p^\rho k^\sigma 2T_1(q^2), \qquad (18)$$

$\langle\varphi(k,\varepsilon)|\bar{s}\sigma_{\mu\nu}\gamma_5 q^\nu b|B_s(p)\rangle$

$$= T_2(q^2)[\varepsilon_\mu^*(M_{B_s}^2 - M_\varphi^2) - (p+k)_\mu(\varepsilon^* \cdot q)]$$

$$+ T_3(q^2)(\varepsilon^* \cdot q)\left[q_\mu - \frac{q^2}{M_{B_s}^2 - M_\varphi^2}(p+k)_\mu\right], \qquad (19)$$

where $\varepsilon^{*\nu}$ is the polarization of the final-state vector meson (φ).

The form factors A_i and T_i are functions of the square of momentum transfer q, and these are not independent of each other. By contracting the above equations with q_μ and making use of the equation of motion, one can write

$$A_3(q^2) = \frac{M_{B_s} + M_\varphi}{2M_\varphi}A_1(q^2) - \frac{M_{B_s} - M_\varphi}{2M_\varphi}A_2(q^2),$$

$$A_3(0) = A_0(0), \qquad T_1(0) = T_2(0). \qquad (20)$$

The form factors for $B_s \to \varphi$ transition are the nonperturbative quantities and are the major candidate the uncertainties. In literature, there exist different approaches (both perturbative and nonperturbative) like lattice QCD, QCD sum rules, light cone sum rules, etc., to calculate them. Here, we will consider the form factors calculated by using the light-cone sum rules approach by Ball and Braun [58]. The form factors V, A_0, and T_1 are parameterized by

$$F(q^2) = \frac{r_1}{1 - q^2/m_R^2} + \frac{r_2}{1 - q^2/m_{\text{fit}}^2}, \qquad (21)$$

while the form factors A_2 and $\tilde{T}_3$ are parameterized as follows:

$$F(q^2) = \frac{r_1}{1 - q^2/m^2} + \frac{r_2}{(1 - q^2/m^2)^2}. \qquad (22)$$

The fit formula for A_1 and T_2 is

$$F(q^2) = \frac{r_2}{1 - q^2/m_{\text{fit}}^2}. \qquad (23)$$

The form factor T_3 can be obtained through the relation

TABLE I. Fit parameters for $B_s \to \varphi$ transition form factors. $F(0)$ denotes the value of form factors at $q^2 = 0$ [cf. Eq. (21)]. The theoretical uncertainty estimated is around 15%.

$F(q^2)$	$F(0)$	r_1	m_R^2	r_2	m_{fit}^2
$A_1(q^2)$	0.311	$\cdots$	$\cdots$	0.308	36.54
$A_2(q^2)$	0.234	-0.054	$\cdots$	0.288	48.94
$A_0(q^2)$	0.474	3.310	5.28^2	-2.835	31.57
$V(q^2)$	0.434	1.484	5.32^2	-1.049	39.52
$T_1(q^2)$	0.349	1.303	5.32^2	-0.954	38.28
$T_2(q^2)$	0.349	$\cdots$	$\cdots$	0.349	37.21
$\tilde{T}_3(q^2)$	0.349	0.027	$\cdots$	0.321	45.56

$$T_3(q^2) = \frac{M_{B_s}^2 - M_\varphi^2}{q^2}[\tilde{T}_3(q^2 - T_2(q^2)],$$

where the values of different parameters are summarized in Table I.

Hence, by using the above given matrix elements, which are parameterized in terms of the form factors, the decay amplitude for $B_s \to \varphi\ell^+\ell^-$ can be written as

$$\mathcal{M} = \frac{\alpha G_F}{4\sqrt{2}\pi}V_{tb}V_{ts}^*[\bar{l}\gamma^\mu(1-\gamma^5)l \times (-2\mathcal{J}_1\epsilon_{\mu\nu\lambda\sigma}\epsilon^{*\nu}k^\lambda q^\sigma$$

$$- i\mathcal{J}_2\epsilon_\mu^* + i\mathcal{J}_3\epsilon^* \cdot q(p+k)_\mu + i\mathcal{J}_4\epsilon^* \cdot qq_\mu)$$

$$+ \bar{l}\gamma^\mu(1+\gamma^5)l \times (-2\mathcal{J}_5\epsilon_{\mu\nu\lambda\sigma}\epsilon^{*\nu}k^\lambda q^\sigma - i\mathcal{J}_6\epsilon_\mu^*$$

$$+ i\mathcal{J}_7\epsilon^* \cdot q(p+k)_\mu + i\mathcal{J}_8\epsilon^* \cdot qq_\mu)]. \qquad (24)$$

Keeping the final-state leptons' mass, we can see that the first line of the above equation will survive only for $\bar{\ell}\gamma^\mu\gamma^5\ell$ due to the fact that $q_\mu(\bar{\ell}\gamma^\mu\gamma^5\ell) = 2m_l(\bar{\ell}\gamma^5\ell)$, and it will vanish for $\bar{l}\gamma^\mu l$ because of $q_\mu(\bar{l}\gamma^\mu l) = 0$.

The auxiliary functions $\mathcal{J}_1, ..., \mathcal{J}_8$ contain both long- and short-distance physics, which are encapsulated in the form factors and in the Wilson coefficients, respectively. These functions can be written in the following form:

$$\mathcal{J}_1 = 2C_{LL}\mathcal{D}_1 + 4m_b C_7^{\text{eff}}\frac{T_1(s)}{s},$$

$$\mathcal{J}_2 = 2C_{LL}\mathcal{D}_3 + \frac{4m_b}{s}C_7^{\text{eff}}\mathcal{D}_4,$$

$$\mathcal{J}_3 = 2C_{LL}\mathcal{D}_6 + 4\frac{m_b C_7^{\text{eff}}}{s}\mathcal{D}_5,$$

$$\mathcal{J}_4 = \frac{2M_\varphi}{s}\mathcal{D}_7 - \frac{4m_b}{s}C_7^{\text{eff}}T_3(s),$$

$$\mathcal{J}_5 = \mathcal{J}_1(C_{LL} \to C_{LR}),$$

$$\mathcal{J}_6 = \mathcal{J}_2(C_{LL} \to C_{LR}),$$

$$\mathcal{J}_7 = \mathcal{J}_3(C_{LL} \to C_{LR}),$$

$$\mathcal{J}_8 = \mathcal{J}_4(C_{LL} \to C_{LR}), \qquad (25)$$

where C_{LL}, C_{LR}, and the $\mathcal{D}$'s are defined as follows:

$$C_{LL} = C'_9 - C'_{10}, \qquad C_{LR} = C'_9 + C'_{10},$$

$$\mathcal{D}_1 = \frac{V(s)}{(M_{B_s} + M_\varphi)}, \qquad \mathcal{D}_3 = (M_{B_s} + M_\varphi)A_1(s),$$

$$\mathcal{D}_4 = (M_{B_s}^2 - M_\varphi^2)T_2(s),$$

$$\mathcal{D}_5 = \left[T_2(s) + \frac{s}{(M_{B_s}^2 - M_\varphi^2)}T_3(s) \right],$$

$$\mathcal{D}_6 = \frac{A_2(s)}{(M_{B_s} + M_\varphi)}, \qquad \mathcal{D}_7 = (A_3 - A_0). \qquad (26)$$

Now, with all the ingredients in hand, the next step is to summarize the formulas of different physical observables.

III. FORMULAS OF PHYSICAL OBSERVABLES

A. Differential decay rate

In order to calculate the polarized branching ratio, as well as the unpolarized and polarized *CP*-violation asymmetries, we first have to find the expression for the differential decay width of $B_s \to \varphi\ell^+\ell^-$ decay. The formula for the double differential decay rate can be written as

$$\frac{d^2\Gamma(B_s \to \varphi\ell^+\ell^-)}{d\cos\theta ds} = \frac{1}{2M_{B_s}^3}\frac{2\beta\sqrt{\lambda}}{(8\pi)^3}|\mathcal{M}|^2, \qquad (27)$$

where $\beta \equiv \sqrt{1 - \frac{4m_l^2}{s}}$ and $\lambda = \lambda(M_{B_s}, M_\varphi, s) \equiv M_{B_s}^4 + M_\varphi^4 + s^2 - 2M_{B_s}^2 M_\varphi^2 - 2sM_{B_s}^2 - 2sM_\varphi^2$. Also, s is just the square of the momentum transfer q, and θ is the angle between the lepton and the final-state meson in the rest frame of B_s. By using the expression of the decay amplitude given in Eq. (24) and integrating on $\cos\theta$, one can get the expression of the dilepton invariant mass spectrum as

$$\frac{d\Gamma(B_s \to \varphi\ell^+\ell^-)}{ds} = \frac{G_F^2\alpha^2\beta\sqrt{\lambda}M_{B_s}}{2^{14}\pi^5}|V_{tb}V_{ts}^*|^2\mathcal{M}_1, \qquad (28)$$

with

$$\mathcal{M}_1 = 4(2m_l^2 + s)\left\{\frac{8\lambda}{3}\mathcal{R}e|\mathcal{J}_1|^2 + \frac{12M_\varphi^2 s + \lambda}{3M_\varphi^2 s}\mathcal{R}e|\mathcal{J}_2|^2 - \frac{(M_{B_s}^2 - M_\varphi^2 - s)}{3M_\varphi^2 s}\lambda\mathcal{R}e(\mathcal{J}_2\mathcal{J}_3^*) + \frac{\lambda^2}{3M_\varphi^2 s}\mathcal{R}e|\mathcal{J}_3|^2\right\}$$

$$+ \frac{32\lambda}{3}(s - 4m_l^2)\mathcal{R}e|\mathcal{J}_5|^2 + \left[\frac{4\lambda(2m_l^2 + s)}{3M_\varphi^2 s} + 16(s - 4m_l^2)\right] \times \mathcal{R}e|\mathcal{J}_6|^2 - \frac{4\lambda}{3M_\varphi^2 s}\{[(2m_l^2 + s)(M_{B_s}^2 - M_\varphi^2)$$

$$+ s(s - 4m_l^2)]\mathcal{R}e(\mathcal{J}_6\mathcal{J}_7^*) + [6m_l^2 s(2M_{B_s}^2 + 2M_\varphi^2 - s) + \lambda(2m_l^2 + s)]\mathcal{R}e|\mathcal{J}_7|^2 + \frac{8m_l^2\lambda}{M_\varphi^2}(M_{B_s}^2 - M_\varphi^2)\mathcal{R}e(\mathcal{J}_7\mathcal{J}_8^*)$$

$$- s\frac{8m_l^2\lambda}{M_\varphi^2}\mathcal{R}e|\mathcal{J}_8|^2\}. \qquad (29)$$

Here we take the liberty to correct the expression of the decay rate given in Ref. [36].

B. Branching ratio of $B_s \to \varphi\ell^+\ell^-$ with polarized φ

The total decay rate for $B_s \to \phi\ell^+\ell^-$ can be written in terms of the longitudinal (Γ_L) and normal components (Γ_T) when the final-state vector meson is polarized. The explicit expressions of the differential decay rate in terms of these components can be written as [59]

$$\frac{d\Gamma(s)}{ds} = \frac{d\Gamma_L(s)}{ds} + \frac{d\Gamma_T(s)}{ds}, \qquad (30)$$

where

$$\frac{d\Gamma_T(s)}{ds} = \frac{d\Gamma_+(s)}{ds} + \frac{d\Gamma_-(s)}{ds}$$

and

$$\frac{d\Gamma_L(s)}{ds} = \frac{G_F^2|V_{tb}V_{ts}^*|^2\alpha^2}{2^{11}\pi^5}\frac{\beta\sqrt{\lambda}}{M_{B_s}^3} \times \frac{1}{3}\mathcal{A}_L, \qquad (31)$$

$$\frac{d\Gamma_\pm(s)}{ds} = \frac{G_F^2|V_{tb}V_{ts}^*|^2\alpha^2}{2^{11}\pi^5}\frac{\beta\sqrt{\lambda}}{M_{B_s}^3} \times \frac{4}{3}\mathcal{A}_\pm. \qquad (32)$$

The different functions appearing in Eqs. (31) and (32) can be written as

$$\mathcal{A}_L = \frac{1}{sM_\varphi^2}[24|\mathcal{K}_7(s)|^2 m_l^2 M_\varphi^2\lambda$$

$$+ (2m_l^2 + s)|(M_{B_s}^2 - M_\varphi^2 - s)\mathcal{K}_2(s) + \lambda\mathcal{K}_3(s)|^2$$

$$+ (s - 4m_l^2)|(M_{B_s}^2 - M_\varphi^2 - s)\mathcal{K}_5(s) + \lambda\mathcal{K}_6(s)|^2], \qquad (33)$$

$$\mathcal{A}_{\pm} = (s - 4m_l^2)|\mathcal{K}_5(s) \mp \sqrt{\lambda}\mathcal{K}_4(s)|^2$$
$$+ (s + 2m_l^2)|\mathcal{K}_2(s) \pm \sqrt{\lambda}\mathcal{K}_1(s)|^2, \quad (34)$$

with

$$\mathcal{K}_1(s) = 4C_7^{\text{eff}}\frac{m_b}{s}T_1(s) + 2C_9'\mathcal{D}_1, \quad (35)$$

$$\mathcal{K}_2(s) = 2\frac{m_b}{s}C_7^{\text{eff}}\mathcal{D}_4 + C_9'\mathcal{D}_3, \quad (36)$$

$$\mathcal{K}_3(s) = 4C_7^{\text{eff}}\mathcal{D}_5 + C_9'\mathcal{D}_6, \quad (37)$$

$$\mathcal{K}_4(s) = 2C_{10}'\mathcal{D}_1, \quad (38)$$

$$\mathcal{K}_5(s) = 2C_{10}'A_0(s)(M_{B_s} + M_{\varphi}), \quad (39)$$

$$\mathcal{K}_6(s) = 2C_{10}'\frac{\mathcal{D}_3}{(M_{B_s} + M_{\varphi})^2}, \quad (40)$$

$$\mathcal{K}_7(s) = 4C_{10}'\mathcal{D}_6. \quad (41)$$

In the above equations, the functions $\mathcal{D}_1, \ldots, \mathcal{D}_6$ are given in Eq. (26).

C. Polarized and unpolarized *CP*-violation asymmetries

The nonequality of the decay rates of a particle and its antiparticle defines the *CP*-violation asymmetry. The *CP*-violation asymmetry arises whether the final-state leptons are unpolarized or polarized. In the case of unpolarized leptons, the normalized *CP*-violation asymmetries can be defined through the difference of the differential decay rates of the particle and antiparticle decay modes as follows [60,61]:

$$\mathcal{A}_{CP}(\mathbf{S}^{\pm} = \mathbf{e}_i^{\pm}) = \frac{\frac{d\Gamma(\mathbf{S}^-)}{ds} - \frac{d\bar{\Gamma}(\mathbf{S}^+)}{ds}}{\frac{d\Gamma}{ds} - \frac{d\bar{\Gamma}}{ds}}, \quad (42)$$

where

$$\frac{d\Gamma(\mathbf{S}^-)}{ds} = \frac{d\Gamma(B_s \to \varphi\ell^+\ell^-(\mathbf{S}^-))}{ds},$$
$$\frac{d\bar{\Gamma}(\mathbf{S}^+)}{ds} = \frac{d\bar{\Gamma}(B_s \to \varphi\ell^+(\mathbf{S}^+))\ell^-}{ds}.$$

The differential decay rate of $B_s \to \varphi\ell^+\ell^-$ is given in Eq. (28); analogously, the *CP* conjugated differential decay width can be written as

$$\frac{d\bar{\Gamma}(\mathbf{S}^{\pm})}{ds} = \frac{1}{2}\left(\frac{d\bar{\Gamma}}{ds}\right)[1 + (P_L\mathbf{e}_L^{\pm} + P_N\mathbf{e}_N^{\pm} + P_T\mathbf{e}_T^{\pm}) \cdot \mathbf{S}^{\pm}].$$

It is noted here that $\frac{d\bar{\Gamma}}{ds}$ belongs to the transition $\bar{B}_s \to \bar{\varphi}\ell^+\ell^-$, which can be obtained by replacing Λ_{sb} with Λ_{sb}^* in Eq. (12). Furthermore, by using the fact that $\mathbf{S}^+ = -\mathbf{S}^-$ for the longitudinal (*L*) and normal (*N*) polarizations, and $\mathbf{S}^+ = \mathbf{S}^-$ for the transverse (*T*) polarizations, we get

$$\mathcal{A}_{CP}(\mathbf{S}^{\pm} = \mathbf{e}_i^{\pm}) = \frac{1}{2}\left[\frac{\left(\frac{d\Gamma}{ds}\right) - \left(\frac{d\bar{\Gamma}}{ds}\right)}{\left(\frac{d\Gamma}{ds}\right) + \left(\frac{d\bar{\Gamma}}{ds}\right)} \pm \frac{\left(\frac{d\Gamma}{ds}\right)P_i - \left\{\left(\frac{d\bar{\Gamma}}{ds}\right)P_i\right\}_{\Lambda_{sb} \to \Lambda_{sb}^*}}{\left(\frac{d\Gamma}{ds}\right) + \left(\frac{d\bar{\Gamma}}{ds}\right)}\right],$$

where i denotes the *L*, *N*, or *T* polarizations of the final-state leptons. By using Eq. (26) in the above equation, the expression of *CP*-violation asymmetry becomes

$$\mathcal{A}_{CP}(\mathbf{S}^{\pm} = \mathbf{e}_i^{\pm}) = \frac{1}{2}\left[\frac{\mathcal{M}_1 - \bar{\mathcal{M}}_1}{\mathcal{M}_1 + \bar{\mathcal{M}}_1} \pm \frac{\mathcal{M}_1^i - \bar{\mathcal{M}}_1^i}{\mathcal{M}_1^i + \bar{\mathcal{M}}_1^i}\right], \quad (43)$$

where $\bar{\mathcal{M}}_1 = (\mathcal{M}_1)_{\Lambda_{sb} \to \Lambda_{sb}^*}$, $\bar{\mathcal{M}}_1^i = (\mathcal{M}_1^i)_{\Lambda_{sb} \to \Lambda_{sb}^*}$, and

$$\mathcal{A}_{CP}(s) = \frac{\mathcal{M}_1 - \bar{\mathcal{M}}_1}{\mathcal{M}_1 + \bar{\mathcal{M}}_1}, \qquad \mathcal{A}_{CP}^i(s) = \frac{\mathcal{M}_1^i - \bar{\mathcal{M}}_1^i}{\mathcal{M}_1^i + \bar{\mathcal{M}}_1^i}. \quad (44)$$

Hence, by using these definitions, the normalized *CP*-violation asymmetry can be written as follows:

$$\mathcal{A}_{CP}(\mathbf{S}^{\pm} = \mathbf{e}_i^{\pm}) = \frac{1}{2}[\mathcal{A}_{CP}(s) \pm \mathcal{A}_{CP}^i(s)], \quad (45)$$

where the plus sign in the second term of the above expression corresponds to the *L* and *N* polarizations, and the negative sign is for the *T* polarization.

The first term in $\mathcal{A}_{CP}(s)$ in Eq. (45) is the unpolarized *CP*-violation asymmetry, while the second term $\mathcal{A}_{CP}^i(s)$ is called the polarized *CP*-violation asymmetry and provides the modifications to the first term. After doing some tedious calculation, we have found the following results for $\mathcal{A}_{CP}(s)$ and $\mathcal{A}_{CP}^i(s)$:

$$\mathcal{A}_{CP}(s) = \frac{-2\mathcal{I}m(\Lambda_{sb})\mathcal{Q}(s)}{\mathcal{M}_1 + 2\mathcal{I}m(\Lambda_{sb})\mathcal{Q}(s)}, \quad (46)$$

$$\mathcal{A}_{CP}^i(s) = \frac{-2\mathcal{I}m(\Lambda_{sb})\mathcal{Q}^i(s)}{\mathcal{M}_1 + 2\mathcal{I}m(\Lambda_{sb})\mathcal{Q}^i(s)}, \quad (47)$$

with $i = L$, N, or T. The explicit expressions of $\mathcal{Q}(s)$ and $\mathcal{Q}^i(s)$ are given below:

$$\mathcal{Q}(s) = \mathcal{H}_1 \mathcal{I}m(C_7 C_9^{*\prime}) + \mathcal{H}_2 \mathcal{I}m(C_9^* C_9'),$$

$$\mathcal{Q}^L(s) = \mathcal{H}_3 \{\mathcal{I}m(C_{10}' C_9^*) + \mathcal{I}m(C_9^{*\prime} C_{10})\},$$

$$\mathcal{Q}^N(s) = \mathcal{H}_4 \mathcal{I}m(C_7 C_9^{*\prime}) + \mathcal{H}_5 \{\mathcal{I}m(C_{10} C_9^{*\prime})\}$$
$$+ \mathcal{H}_6 \mathcal{I}m(C_9^* C_9'),$$

$$\mathcal{Q}^T(s) = \frac{\beta}{2} \mathcal{H}_6 \{\mathcal{R}e(C_{10} C_9^{*\prime}) + \mathcal{R}e(C_{10}' C_9^*)\}. \tag{48}$$

The functions $\mathcal{H}_1, \ldots, \mathcal{H}_6$ can be written as

$$\mathcal{H}_1 = \frac{64}{3 M_\varphi^2 s} M_{B_s} [(\mathcal{D}_3 \mathcal{D}_5 + \mathcal{D}_6 \mathcal{D}_4)\lambda(M_\varphi^2 - M_{B_s}^2 + s)$$
$$+ (\mathcal{D}_3 \mathcal{D}_4 + \mathcal{D}_5 \mathcal{D}_6)\lambda + (3\mathcal{D}_3 \mathcal{D}_4 + 2\mathcal{D}_1 F_1(s)\lambda)],$$

$$\mathcal{H}_2 = \frac{32(2 m_l + s)^2}{3 M_\varphi^2 s} [2\mathcal{D}_3 \mathcal{D}_6 \lambda(M_\varphi^2 - M_{B_s}^2 + s)$$
$$+ 8\mathcal{D}_1^2 M_\varphi^2 s\lambda + \mathcal{D}_3^2(12 M_\varphi^2 s + \lambda) + \mathcal{D}_6^2 \lambda^2],$$

$$\mathcal{H}_3 = \frac{32\beta}{3 M_\varphi^2} [2\lambda(M_{B_s}^2 - M_\varphi^2 - s)\mathcal{D}_3 \mathcal{D}_6$$
$$- \mathcal{D}_3^2(12 M_\varphi^2 s + \lambda) - \lambda(8 M_\varphi^2 s \mathcal{D}_1^2 + \lambda \mathcal{D}_6^2)],$$

$$\mathcal{H}_4 = \frac{128\pi}{\sqrt{s}} m_l M_{B_s} \sqrt{\lambda} [F_1(s)\mathcal{D}_3 + \mathcal{D}_1 \mathcal{D}_4],$$

$$\mathcal{H}_5 = \frac{8\pi m_l \sqrt{\lambda}}{M_\varphi^2 \sqrt{s}} (\mathcal{D}_6(M_\varphi^2 - M_{B_s}^2) + \mathcal{D}_3 - 2\sqrt{s}\mathcal{D}_7)$$
$$\times (\mathcal{D}_3(M_\varphi^2 - M_{B_s}^2 + s) + \mathcal{D}_6 \lambda),$$

$$\mathcal{H}_6 = 128 m_l \pi \sqrt{\lambda s} \mathcal{D}_1 \mathcal{D}_3. \tag{49}$$

Here we would like to mention that the functions $\mathcal{H}_4$, $\mathcal{H}_5$, and $\mathcal{H}_6$ are proportional to the mass of the final-state lepton; therefore, their contribution is small when we have μ's as final state leptons compared to that when we have τ's.

IV. NUMERICAL ANALYSIS

In this section, we will give a phenomenological analysis of the polarized branching ratio, when the final-state φ meson is longitudinal (transverse) polarized [$\mathcal{BR}_L$ ($\mathcal{BR}_T$)], as well as of the unpolarized and polarized CP-violation asymmetries for $B_s \to \varphi \ell^+ \ell^-$ decay. In order to see the impact of the new Z' boson on the these physical observables, first we have summarized the numerical values of various input parameters such as masses of particles, lifetimes, CKM matrix elements, etc., in Table II, while the values of Wilson coefficients in the SM are displayed in Table III. The most important input parameters are the form factors which are the nonperturbative quantities, and for them we rely on the light-cone sum rule (LCSR) approach. The numerical values of the LCSR form factors along with the different fitting parameters [58] are summarized in Table I.

TABLE II. Default values of input parameters used in the calculations.

$M_{B_s} = 5.366$ GeV, $m_b = 4.28$ GeV, $m_s = 0.13$ GeV, $m_\mu = 0.105$ GeV, $m_\tau = 1.77$ GeV, $f_{B_s} = 0.25$ GeV, $|V_{tb} V_{ts}^*| = 45 \times 10^{-3}$, $\alpha^{-1} = 137$, $G_F = 1.17 \times 10^{-5}$ GeV^{-2}, $\tau_B = 1.54 \times 10^{-12}$ sec, $M_\varphi = 1.020$ GeV.

TABLE III. The Wilson coefficients C_i^μ at the scale $\mu \sim m_b$ in the SM [48].

C_1	C_2	C_3	C_4	C_5	C_6	C_7	C_9	C_{10}
1.107	−0.248	−0.011	−0.026	−0.007	−0.031	−0.313	4.344	−4.669

Now, the next step is to collect the values of the Z' couplings, and in this regard, there are some severe constraints from different inclusive and exclusive B decays [62]. These numerical values of the coupling parameters of the Z' model are recollected in Table IV, where $\mathcal{S}1$ and $\mathcal{S}2$ correspond to two different fitting values for B_s–$\bar{B}_s$ mixing data collected by the UTfit Collaboration [63].

Motivated by the latest results on the CP-violating phase φ_S^L and the like-sign dimuon charge asymmetry $A_{\rm SL}^b$ of the semileptonic decays given in Refs. [68]. The main emphasis of the study is to check if a simultaneous explanation for all mixing observables, especially of like-sign dimuon asymmetry $A_{\rm SL}^b$, could be made in the Z' model. It has been found that it is not possible to accommodate all the data simultaneously, and the new constraints on the CP-violating phase φ_S and $|\mathcal{B}_{sb}|$ are obtained from ΔM_S, φ_S, $\Delta \Gamma_S$ data. In addition, the constraints on $S_{\ell\ell}^L$ and $S_{\ell\ell}^R$ are obtained from the analysis of $B \to X_s \mu^+ \mu^-$ [69], $B \to K^* \mu^+ \mu^-$ [70,71], and $B \to \mu^+ \mu^-$ [72]. In the forthcoming study, this is referred to as scenario $\mathcal{S}3$. The corresponding numerical values are chosen from Refs. [68,73], and these are summarized in Table IV.

Just to mention again, $\mathcal{B}_{sb} = |\mathcal{B}_{sb}| e^{-i\varphi_{sb}}$ is the off-diagonal left-handed coupling of the Z' boson with quarks, and φ_{sb} corresponds to a new weak phase, whereas S_{LL} and D_{LL} represent the combination of left- and right-handed couplings of Z' with the leptons [cf. Eq. (13)]. In order to fully scan the three scenarios, let us remark that with

TABLE IV. The numerical values of the Z' parameters [62,63,68,73].

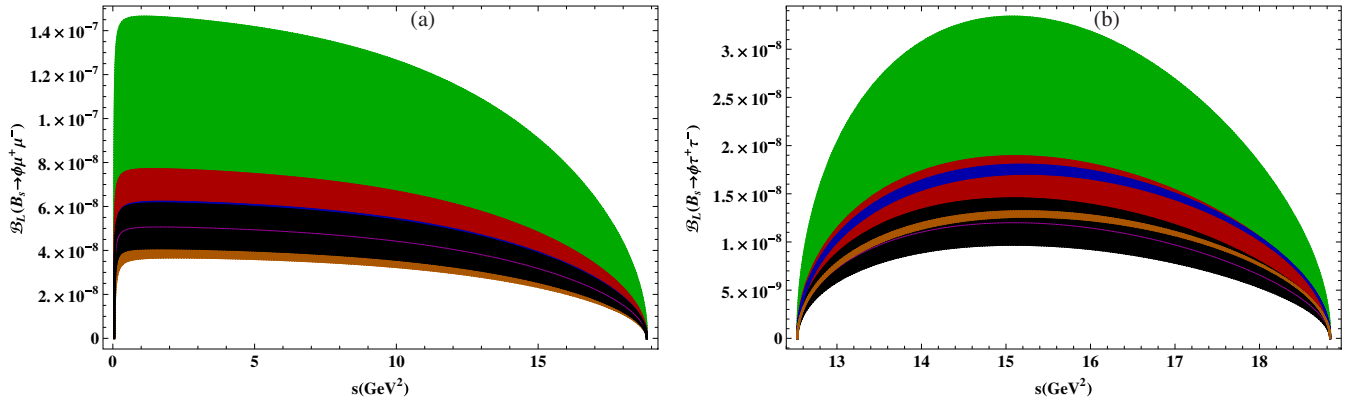|	$|\mathcal{B}_{sb}| \times 10^{-3}$	φ_{sb} (in degrees)	$S_{LL} \times 10^{-2}$	$D_{LL} \times 10^{-2}$
$\mathcal{S}1$	1.09 ± 0.22	-72 ± 7	-2.8 ± 3.9	-6.7 ± 2.6
$\mathcal{S}2$	2.20 ± 0.15	-82 ± 4	-1.2 ± 1.4	-2.5 ± 0.9
$\mathcal{S}3$	4.0 ± 1.5	150 ± 10 or (-150 ± 10)	0.8	-2.6

FIG. 1 (color online).   Longitudinal polarized branching ratio $\mathcal{BR}_L$ as a function of the square of momentum s for $B_s \rightarrow \varphi \mu^+ \mu^-$ [(a)] and $B_s \rightarrow \varphi \tau^+ \tau^-$ (b)] for scenarios $\mathcal{S}1$, $\mathcal{S}2$, and $\mathcal{S}3$. The green and red colors correspond to the $\mathcal{S}1$ and $\mathcal{S}2$, respectively. The blue and orange colors show $\mathcal{S}3$. The band in each case depicts the variations of φ_{sb} in respective scenarios. The black color corresponds to the SM results where the band is due to uncertainties in different input parameters.

$D_{LL} \neq 0$, we depict the situation when the new physics comes only from the modification in the Wilson coefficient C_{10}, while the opposite case, $S_{LL} \neq 0$, indicates that the new physics is due to the change in the Wilson coefficient

C_9 [see Eq. (13)]. In Figs. 1–4, we have displayed the results of the branching ratio when the final-state meson (φ) is polarized. Figures 1 and 3 represent the cases where $\mathcal{BR}_L$ and $\mathcal{BR}_T$ are plotted as a function of s by taking the
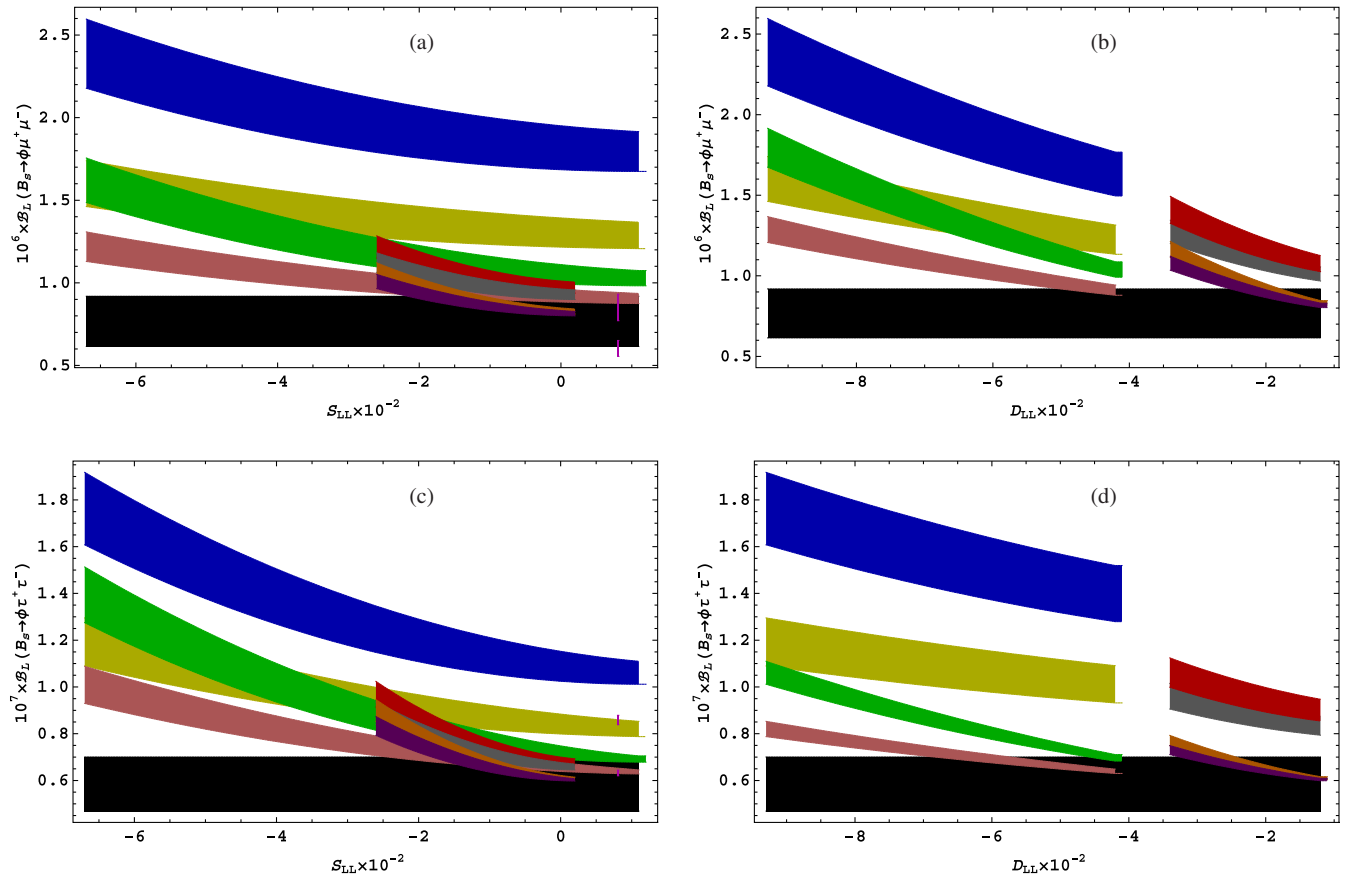

FIG. 2 (color online).   Longitudinal polarized branching ratio $\mathcal{BR}_L$ as a function of the square of momentum D_{LL} and S_{LL} for $B_s \rightarrow \varphi \mu^+ \mu^-$ [(a,b)] and $B_s \rightarrow \varphi \tau^+ \tau^-$ [(c,d)] for scenarios $\mathcal{S}1$ and $\mathcal{S}2$. The blue, yellow, green, and dark pink colors correspond to the $\mathcal{S}1$ where as the other colors are for the $\mathcal{S}2$. The vertical magenta color bars corresponding to the $\mathcal{S}3$ scenario. The band in each case depicts the variations of φ_{sb} in the respective scenario. The black band corresponds to the SM results where the band is due to uncertainty in different input parameters.
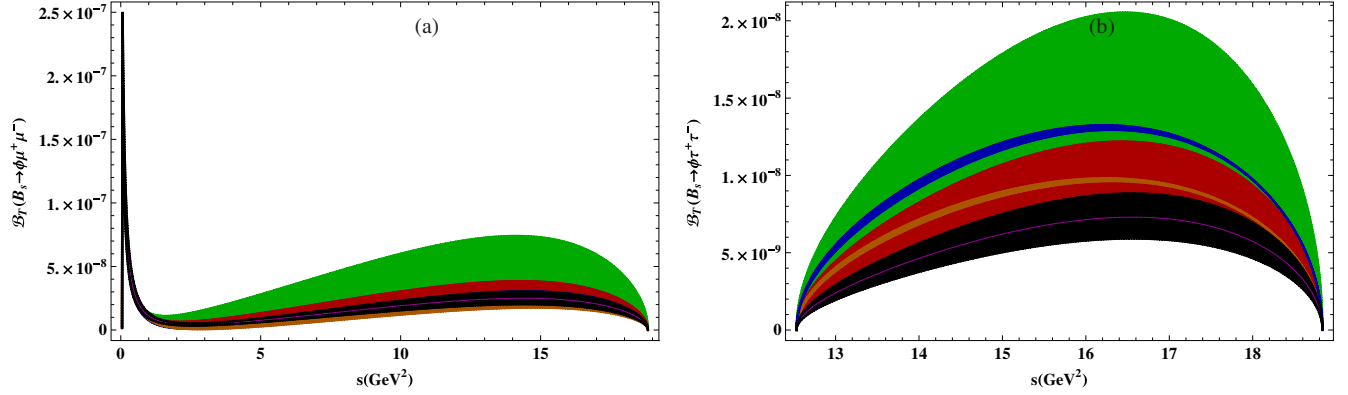
FIG. 3 (color online). Transverse polarized branching ratio $\mathcal{BR}_T$ as a function of the square of momentum s for $B_s \to \varphi\mu^+\mu^-$ [(a)] and $B_s \to \varphi\tau^+\tau^-$ [(b)] for scenarios $\mathcal{S}1$, $\mathcal{S}2$, and $\mathcal{S}3$. The green and red colors correspond to the $\mathcal{S}1$ and $\mathcal{S}2$, respectively. The blue and orange colors show the $\mathcal{S}3$. The band in each case depicts the variations of φ_{sb} in the respective scenarios. The black color corresponds to the SM results where the band is due to uncertainties in different input parameters.

values of different Z' parameters given in Table IV. In Figs. 2 and 4, the average normalized polarized branching ratios, after integration on s, as a function of S_{LL} and D_{LL}, are depicted. In the same way, the averaged CP-violation asymmetry as a function of S_{LL} and D_{LL} is shown in

Figs. 5–12. The different color combinations, along with the corresponding values of Z' parameters, are summarized in Table V. Likewise, in scenario $\mathcal{S}3$, the values of the Z' parameters are summarized in Table IV, and their color codes in different figures are given in Eq. (50):
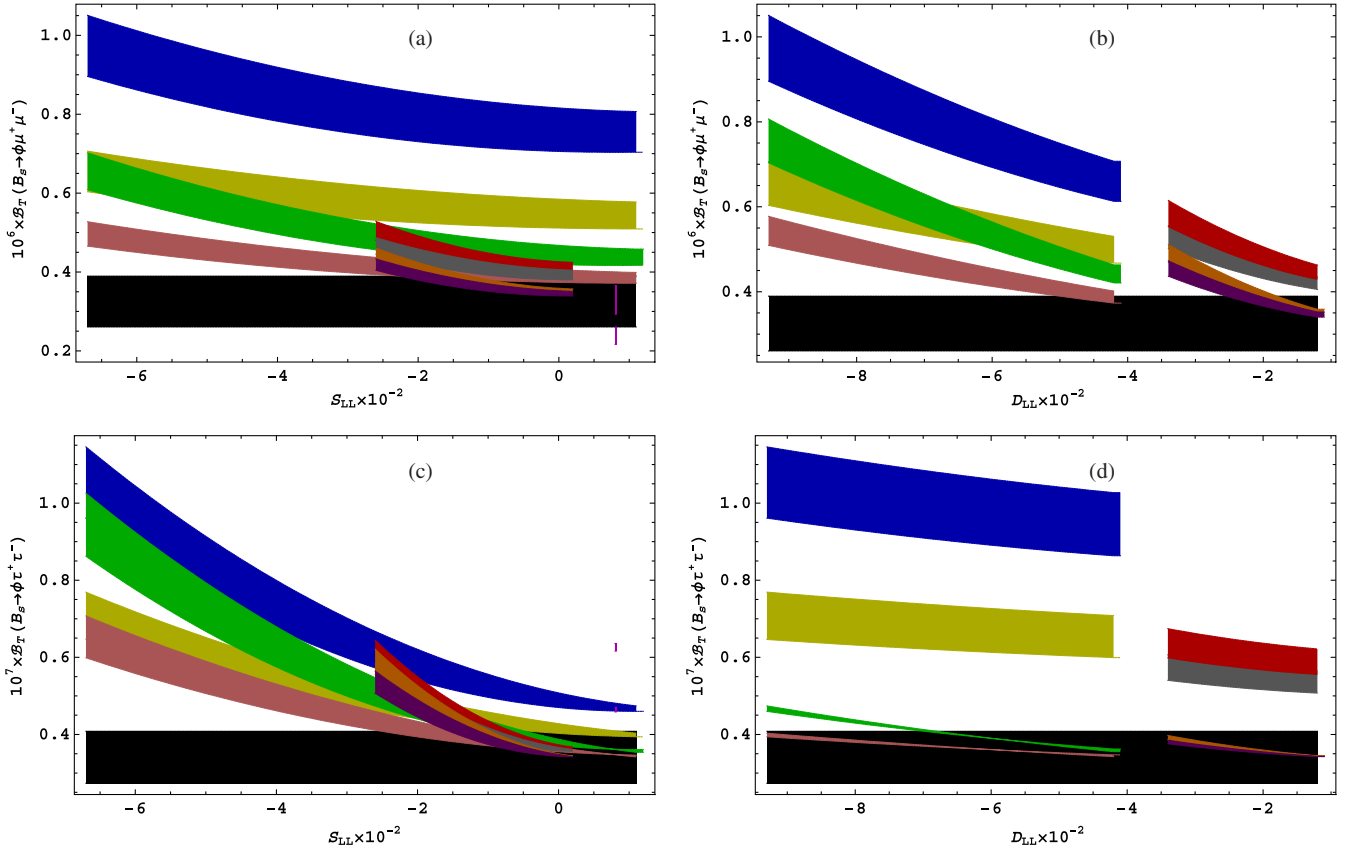

FIG. 4 (color online). The transverse lepton polarization asymmetry for the $B_s \to \varphi l^+ l^-$ ($l = \mu, \tau$) decays as functions of Z' parameters. The legends are same as in Fig. 2.
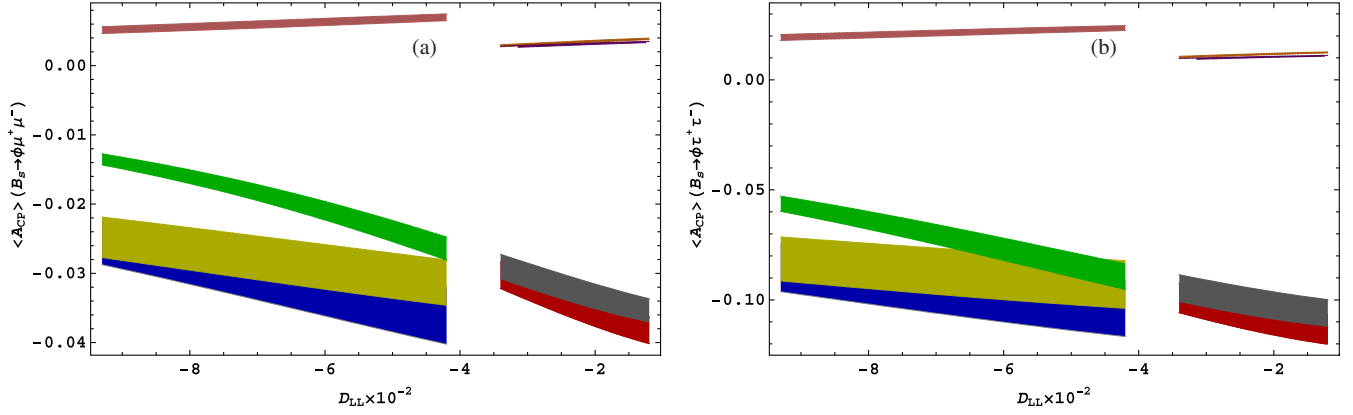
FIG. 5 (color online).   Unpolarized CP-violation asymmetry $\mathcal{A}_{CP}$ as a function of D_{LL} for $B_s \to \varphi\mu^+\mu^-$ and [(a)] $B_s \to \varphi\tau^+\tau^-$ for scenarios $\mathcal{S}1$ and $\mathcal{S}2$. The blue, yellow, green, and dark pink colors correspond to $\mathcal{S}1$, whereas the other colors are for $\mathcal{S}2$. The band in each case depicts the variations of φ_{sb} in the respective scenario.

$$|\mathcal{B}_{sb}| = 3 \times 10^{-3}: \begin{cases} \varphi_{sb} = 160^{\circ}, \text{ Red dot} \\ \varphi_{sb} = 140^{\circ}, \text{ Blue dot} \\ \varphi_{sb} = -140^{\circ}, \text{ Green dot} \\ \varphi_{sb} = -160^{\circ}, \text{ Gray dot} \end{cases};$$

$$|\mathcal{B}_{sb}| = 5 \times 10^{-3}: \begin{cases} \varphi_{sb} = 160^{\circ}, \text{Orange dot} \\ \varphi_{sb} = 140^{\circ}, \text{Yellow dot} \\ \varphi_{sb} = -140^{\circ}, \text{Pink dot} \\ \varphi_{sb} = -160^{\circ}, \text{Purple dot} \end{cases}. \qquad (50)$$

A. Longitudinal polarized branching ratio $\mathcal{BR}_L$

In Figs. 1(a) and 1(b), we have plotted the branching ratio when the final-state φ is longitudinally polarized, named the longitudinal polarized branching ratio ($\mathcal{BR}_L$), as a function of s for μ and τ as final-state leptons in $B_s \to \varphi\ell^+\ell^-$ decay. By looking at Eq. (33) it can be seen that $\mathcal{BR}_L$ it is directly proportional to the contributions coming from Z' in C'_{10} encoded in $\mathcal{K}_5$, $\mathcal{K}_6$, and $\mathcal{K}_7$. Apart from this,

it also contains the terms that involve C'_9, which comes in $\mathcal{K}_2$ and $\mathcal{K}_7$, where the latter are m_l suppressed. In Fig. 1, we can see a significant enhancement in $\mathcal{BR}_L$ for the maximum values of Z' parameters, and the results are quite distinct from the SM for both the μ and τ cases.

To see the explicit dependence on the Z' parameters, we have integrated $\mathcal{BR}_L$ on s and have drawn it against D_{LL} and S_{LL} in Figs. 2(a)–2(d). These graphs depict that for $\varphi_{sb} = -79^{\circ}$, $\mathcal{B}_{sb} = 1.31 \times 10^{-3}$, $D_{LL} = -9.3 \times 10^{-2}$, and $S_{LL} = -6.7 \times 10^{-2}$ in scenario $\mathcal{S}1$ (blue band), the increment in the $\mathcal{BR}_L$ is around 3 times in the case of μ and 2.5 times in the case of τ leptons. When decreasing the values of D_{LL} and S_{LL}, the values of integrated $\mathcal{BR}_L$ decreases, and Fig. 2 displays this trend. Compared to the scenario $\mathcal{S}1$, the change in $\mathcal{BR}_L$ is small in $\mathcal{S}2$.

Keeping in view that in scenario $\mathcal{S}3$ the values of S_{LL} and D_{LL} are fixed, we plot two vertical (magenta) bars which correspond to the variation in φ_{sb} and $\mathcal{B}_{sb}$. It can be seen from Figs. 2(a) and 2(c) that in a certain range of parameters of $\mathcal{S}3$, the Z' boson effects are noticeable in $B_s \to$

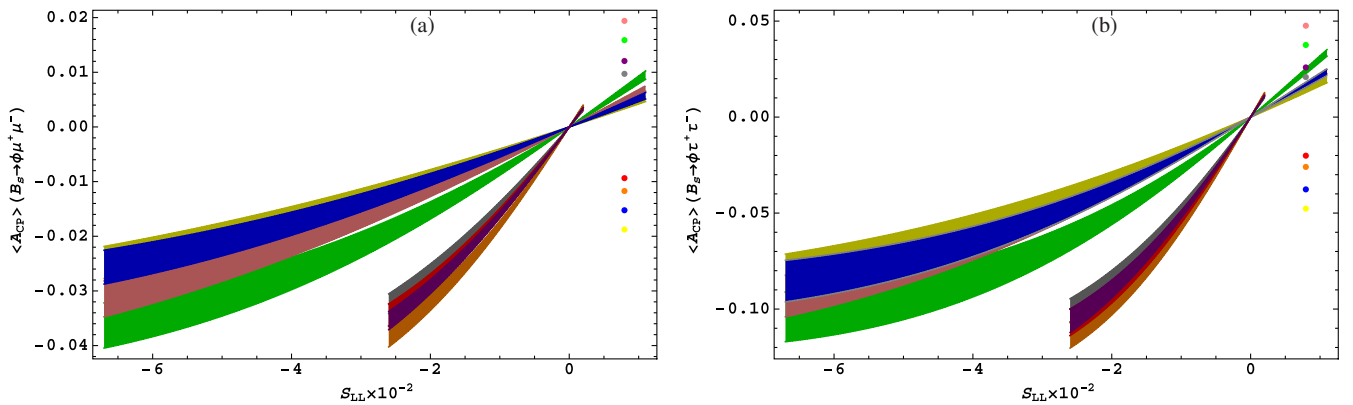
FIG. 6 (color online).   Unpolarized CP-violation asymmetry $\mathcal{A}_{CP}$ as a function of S_{LL} for $B_s \to \varphi\mu^+\mu^-$ [(a)] and $B_s \to \varphi\tau^+\tau^-$ [(b)] for scenarios $\mathcal{S}1$, $\mathcal{S}2$, and $\mathcal{S}3$. The color and band description is the same as in Fig. 5. The different color dots correspond to the different values of Z' parameters in scenario $\mathcal{S}3$.
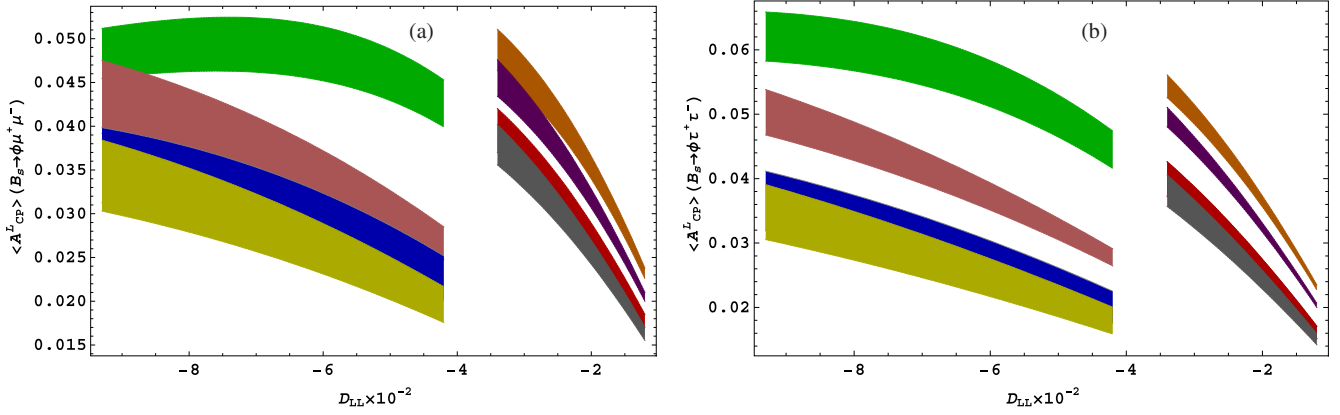
FIG. 7 (color online).   Longitudinal polarized CP-violation asymmetry $\mathcal{A}_{CP}^{L}$ as a function of D_{LL} for $B_s \to \varphi\mu^+\mu^-$ [(a)] and $B_s \to \varphi\tau^+\tau^-$ [(b)] for scenarios $\mathcal{S}1$ and $\mathcal{S}2$. The color and band description is the same as in Fig. 5.

$\varphi\tau^+\tau^-$ decay. Similar bars can be plotted in Figs. 2(b) and 2(d), but they do not add any new information; therefore, we will show the $\mathcal{S}3$ contribution only when different asymmetries are plotted against S_{LL}.

B. Transverse polarized branching ratio $\mathcal{BR}_T$

It can be noticed from Eq. (34) that the transverse polarized branching ratio ($\mathcal{BR}_T$) depends on the functions $\mathcal{K}_1(s)$, $\mathcal{K}_2(s)$, $\mathcal{K}_4(s)$, and $\mathcal{K}_5(s)$ given in Eqs. (35), (36), (38) and (39), respectively. Here, the first two functions $[\mathcal{K}_1(s), \mathcal{K}_2(s)]$ depend on the Wilson coefficients C_7^{eff}, C_9', and the later two on C_{10}'. Therefore, we are expecting quite visible hints of NP coming from the the extra neutral boson Z', and Figs. 3(a) and 3(b), where $\mathcal{BR}_T$ is plotted as a function of s, display this fact. Here, one can clearly distinguish between the values of $\mathcal{BR}_T$ calculated in SM and the Z' scenarios $\mathcal{S}1$, $\mathcal{S}2$, and $\mathcal{S}3$.

To see how $\mathcal{BR}_T$ evolves with the parameters of the Z' model, we have plotted the integrated $\mathcal{BR}_T$ as a function of S_{LL} and D_{LL} in Figs. 4(a)–4(d). Just like $\mathcal{BR}_L$, $\mathcal{BR}_T$

becomes almost 3 times its SM value when $\varphi_{sb} = -79^{\circ}$, $\mathcal{B}_{sb} = 1.31 \times 10^{-3}$, $D_{LL} = -9.3 \times 10^{-2}$, and $S_{LL} = -6.7 \times 10^{-2}$ in scenario $\mathcal{S}1$ (blue band), for both μ and τ leptons. However, these values decreases when the magnitude of S_{LL} decreases, and this is clear from Figs. 4(a) and 4(c). The situation is similar when we plot $\mathcal{BR}_T$ as a function of D_{LL} by fixing the parameters $\mathcal{B}_{sb}$, φ_{sb}, S_{LL} in the range given in Table IV, where one can see that it is also a decreasing function of D_{LL}. However, even for small values of the Z' parameters, the value of the observable is quite distinct from the SM result, especially in scenario $\mathcal{S}1$. Just like the longitudinal polarized branching ratio, the effects of the Z' boson corresponding to scenario $\mathcal{S}3$ [the magenta bar in Fig. 4(c)] in the transverse polarized branching ratio are quite promising in $B_s \to \varphi\tau^+\tau^-$ decay.

C. Unpolarized CP-violation asymmetry

In Figs. 5, and 6 the unpolarized CP-violation asymmetries for $B_s \to \varphi\mu^+\mu^-(\tau^+\tau^-)$ are presented as a function of D_{LL} and S_{LL}. It is well known that in SM the CP-violation
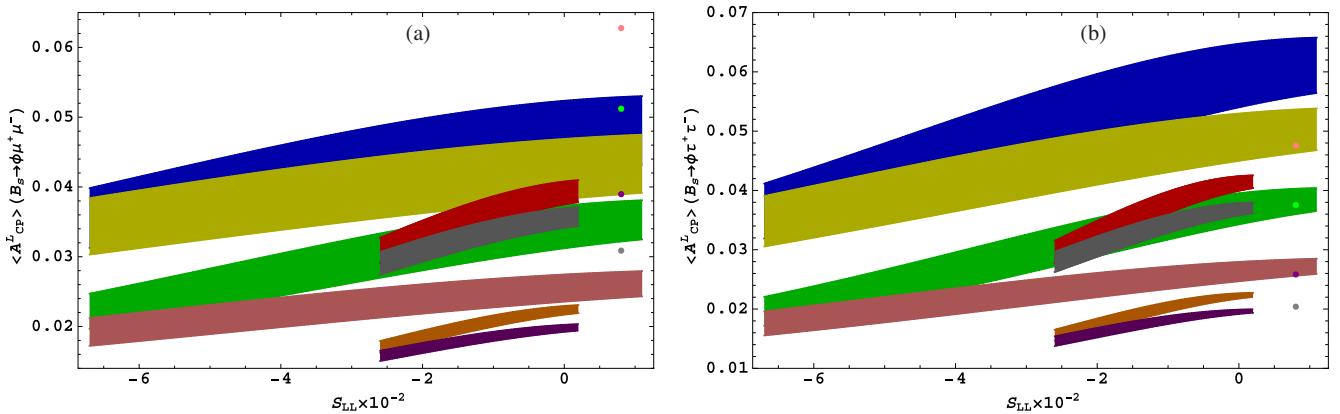

FIG. 8 (color online).   Longitudinal polarized CP-violation asymmetry $\mathcal{A}_{CP}^{L}$ as a function of S_{LL} for $B_s \to \varphi\mu^+\mu^-$ [(a)] and $B_s \to \varphi\tau^+\tau^-$ [(b)] for scenarios $\mathcal{S}1$ and $\mathcal{S}2$. The color and band description is the same as in Fig. 5. The different colored dots correspond to the different values of Z' parameters in scenario $\mathcal{S}3$.
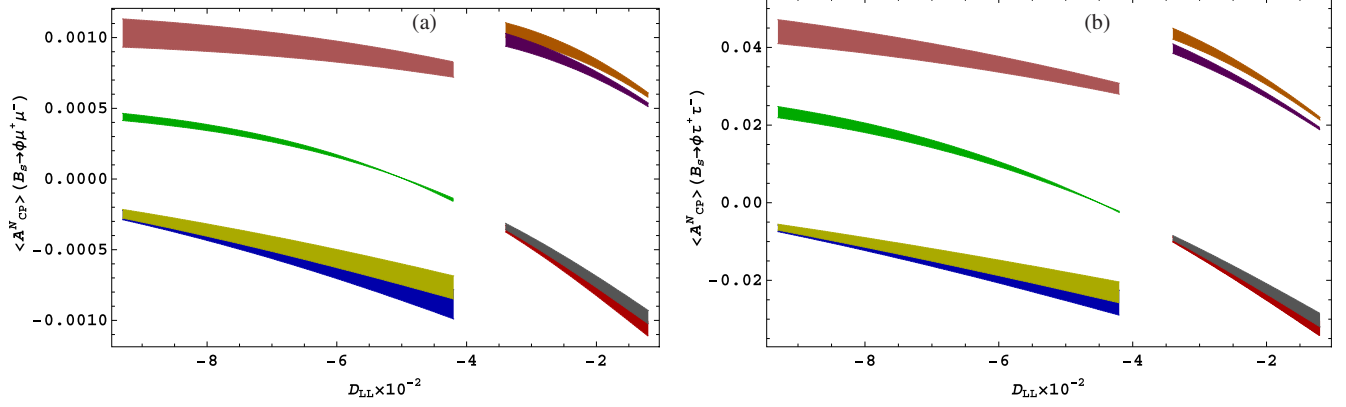
FIG. 9 (color online).   Normal polarized *CP*-violation asymmetry $\mathcal{A}_{CP}^N$ as a function of D_{LL} for $B_s \rightarrow \varphi\mu^+\mu^-$ [(a)] and $B_s \rightarrow \varphi\tau^+\tau^-$ [(b)] for scenarios $\mathcal{S}1$ and $\mathcal{S}2$. The color and band description is the same as in Fig. 5.

asymmetry is almost zero, whereas, by looking at Eq. (46), one can see that $\mathcal{A}_{CP}$ is proportional to the parameters of the Z' model which comes through the imaginary part of the Wilson coefficients, as well as that of the new weak phase φ_{sb} which is encoded in Λ_{sb}. Hence, a significant nonzero value gives us the clear indications of NP arising due to the extra neutral Z' boson. Therefore, we are expecting a dependence on the new phase φ_{sb}, and it is clear from Figs. 5 and 6 where each colored band depicts it. In Fig. 5, by changing the values of S_{LL}, φ_{sb}, and $\mathcal{B}_{sb}$, $\mathcal{A}_{CP}$ is plotted vs D_{LL}, and we can see that the value is not appreciably changed when we have the muon as the final-state lepton. However, in the case of tau leptons [cf. Fig. 5(b)], the value of $\mathcal{A}_{CP}$ is around -0.11 in scenario $\mathcal{S}1$ ($\mathcal{S}2$) for $D_{LL} = -4.1 \times 10^{-2}$ (-1.6×10^{-2}) and $S_{LL} = -6.7 \times 10^{-2}$ (-2.6×10^{-2}), shown by blue (red) bands.

Figure 6 presents the behavior of $\mathcal{A}_{CP}$ with S_{LL} by varying the values of D_{LL}, φ_{sb}, and $\mathcal{B}_{sb}$ in the range given in Table IV. Again, it can be seen that in case of the muon, the value is small compared to the case in which τ's are the final-state leptons. In both cases, $\mathcal{A}_{CP}$ is an increasing

function of S_{LL}. In $B_s \rightarrow \varphi\tau^+\tau^-$, the value of unpolarized *CP* asymmetry is around -0.12 for certain values of Z' parameters in both $\mathcal{S}1$ and $\mathcal{S}2$.

The values of unpolarized *CP*-violation asymmetry in scenario $\mathcal{S}3$ for $B_s \rightarrow \varphi\mu^+\mu^-$ and $B_s \rightarrow \varphi\tau^+\tau^-$ are shown by different colored dots in Figs. 6(a) and 6(b), respectively. It can be noticed that the value of unpolarized *CP*-violation asymmetry is maximum in this scenario when $\varphi_{sb} = 160°$, $|\mathcal{B}_{sb}| = 5 \times 10^{-3}$, and it is depicted by the orange dots in these figures. When the new weak phase (φ_{sb}) has a negative value, the value of the unpolarized *CP*-violation asymmetry is just opposite to the case in which φ_{sb} is positive. This is shown by the lower four dots in Figs. 6(a) and 6(b).

D. Longitudinal polarized *CP*-violation asymmetry

The longitudinal polarized *CP*-violation asymmetry $\mathcal{A}_{CP}^L$ is drawn in Figs. 7 and 8. From Eq. (48) it can be noticed that $\mathcal{Q}^L$ is proportional to the imaginary part of the combination of Wilson coefficients C_9 and C_{10} both in the SM as well as in the Z' model. This makes $\mathcal{A}_{CP}^L$ sensitive to the
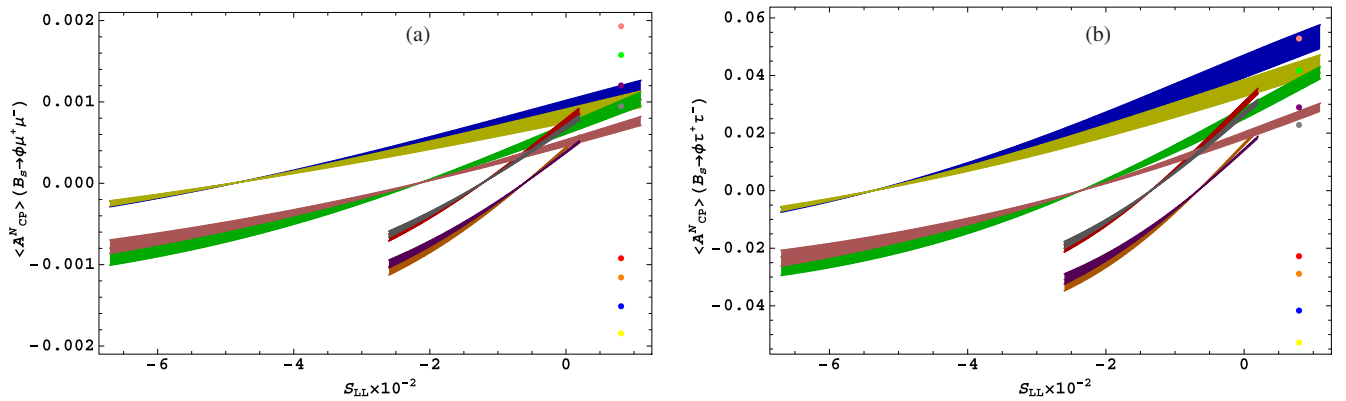

FIG. 10 (color online).   Normal polarized *CP*-violation asymmetry $\mathcal{A}_{CP}^N$ as a function of S_{LL} for $B_s \rightarrow \varphi\mu^+\mu^-$ [(a)] and $B_s \rightarrow \varphi\tau^+\tau^-$ [(b)] for scenarios $\mathcal{S}1$ and $\mathcal{S}2$. The color and band description is the same as in Fig. 5. The different color dots correspond to the different values of Z' parameters in scenario $\mathcal{S}3$.
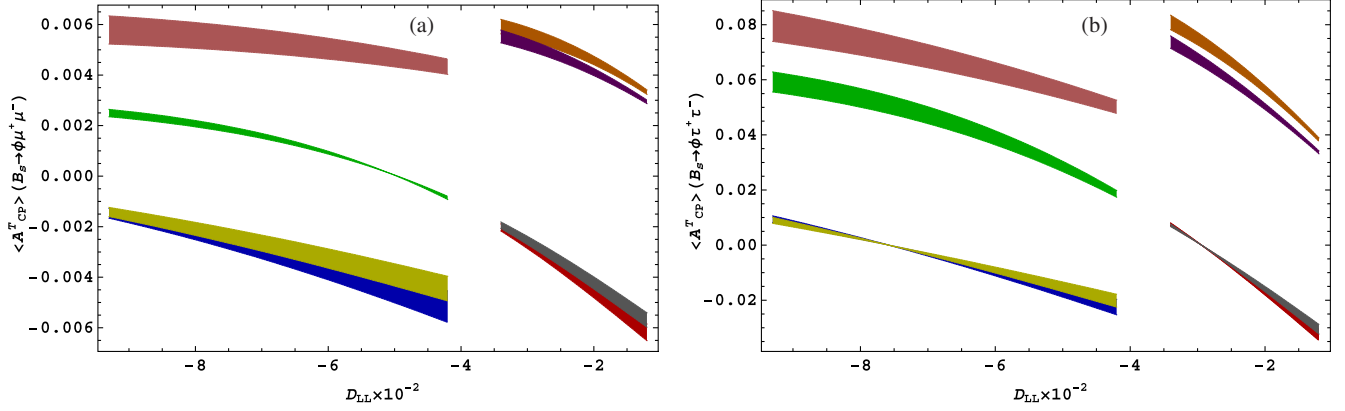
FIG. 11 (color online). Transverse polarized CP-violation asymmetry $\mathcal{A}_{CP}^N$ as a function of D_{LL} for $B_s \to \varphi\mu^+\mu^-$ [(a)] and $B_s \to \varphi\tau^+\tau^-$ [(b)] for scenarios $\mathcal{S}1$ and $\mathcal{S}2$. The color and band description is the same as in Fig. 5.

change in the values of these Wilson coefficients in the Z' model. In Figs. 7(a) and 7(b), we have plotted $\mathcal{A}_{CP}^L$ vs D_{LL} by fixing the values of S_{LL} and other Z' parameters in the range given in Table IV. We can see that the value of $\mathcal{A}_{CP}^L$ increases from 0.015 to 0.055 when muons are the final-state leptons and from 0.018 to 0.068 in case of taus as final-state leptons, which can be visualized from the green (orange) band that corresponds to scenario $\mathcal{S}1$ ($\mathcal{S}2$). The situation when the longitudinal polarized CP-violation asymmetry is plotted with S_{LL} by taking other parameters in the range given in Table IV is displayed in Fig. 8. Here we can see that it is an increasing function of S_{LL}, where in $\mathcal{S}1$ the value increases from 0.040 (0.042) to 0.052 (0.064) when we have $\mu^+\mu^-$ ($\tau^+\tau^-$) final-state leptons, and this is clearly visible from the blue band. In comparison, for $\mathcal{S}2$, these values increase from 0.028 to 0.036 for both μ and τ leptons. It can also be seen in Fig. 8 that the value of longitudinal polarized CP-violation asymmetry in scenario $\mathcal{S}3$ lies in the ballpark of the first two scenarios except for the limit when $\varphi_{sb} = 160°$, $|\mathcal{B}_{sb}| = 5 \times 10^{-3}$. For this value, one can see that the value of longitudinal polarized

CP-violation asymmetry in $B_s \to \varphi\mu^+\mu^-$ is around 0.061, which is significantly different from its value in $\mathcal{S}1$ and $\mathcal{S}2$. Hence, by measuring $\mathcal{A}_{CP}^L$, one can not only segregate the NP coming through the Z' boson but can also distinguish between the three scenarios named here as $\mathcal{S}1$, $\mathcal{S}2$, and $\mathcal{S}3$.

E. Normal polarized CP-violation asymmetry

In contrast to $\mathcal{A}_{CP}$ and $\mathcal{A}_{CP}^L$, the normal polarized CP-violation asymmetry is an order of magnitude smaller in the case of the muon compared to the tauon as the final-state lepton. Let us try to understand it from the expressions presented in Eq. (48). $\mathcal{A}_{CP}^N$ comes from the function $\mathcal{Q}^N$, which contains $\mathcal{H}_4$, $\mathcal{H}_5$, and $\mathcal{H}_6$. In Eq. (49) it is clear that these are proportional to the lepton mass, and their suppression in the case of the muon is obvious, and Figs. 9(a) and 10(a) depict this fact. Coming to Figs. 9(b) and 10(b), we can see that $\mathcal{A}_{CP}^N$ is very sensitive to the parameters of Z' both in $\mathcal{S}1$ and $\mathcal{S}2$, where, similarly to $\mathcal{A}_{CP}$, it changes its sign. In Fig. 9(b), the value of $\mathcal{A}_{CP}^N$ decreases from 0.042 to -0.018 in the parameter range of Z' in $\mathcal{S}1$ and from 0.043 to -0.014 in $\mathcal{S}2$. In contrast, Fig. 10(b) depicts
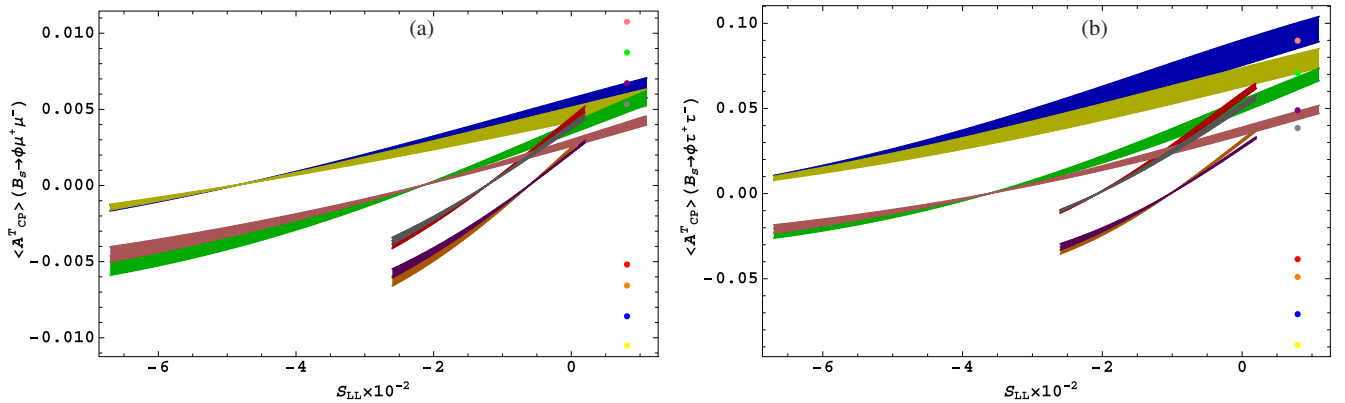

FIG. 12 (color online). Transverse polarized CP-violation asymmetry $\mathcal{A}_{CP}^N$ as a function of S_{LL} for $B_s \to \varphi\mu^+\mu^-$ [(a)] and $B_s \to \varphi\tau^+\tau^-$ [(b)] for scenarios $\mathcal{S}1$ and $\mathcal{S}2$. The color and band description is the same as in Fig. 5. The different color dots correspond to the different values of Z' parameters in scenario $\mathcal{S}3$.

TABLE V. Color bands for Figs. 1–12 $\langle \mathcal{BR}_{L,T} \rangle$, $\langle A_{CP} \rangle$, and $\langle \mathcal{A}^i_{CP} \rangle$ vs S_{LL} and D_{LL} for scenarios $\mathcal{S}1$ and $\mathcal{S}2$.

Color region	φ_{sb}	$\lvert \mathcal{B}_{sb} \rvert \times 10^{-3}$	$\langle \mathcal{BR}_{L,T} \rangle$, $\langle A_{CP} \rangle$, and $\langle \mathcal{A}^i_{CP} \rangle$ vs $S_{LL}D_{LL} \times 10^{-2}$	$\langle \mathcal{BR}_{L,T} \rangle$, $\langle A_{CP} \rangle$, and $\langle \mathcal{A}^i_{CP} \rangle$ vs $D_{LL}S_{LL} \times 10^{-2}$
Blue	$-79°$ $-65°$	$+1.31$	-9.3	-6.7
Red	$-86°$ $-78°$	$+2.35$	-2.34	-2.6
Yellow	$-79°$ $-65°$	$+0.87$	-9.3	-6.7
Black	$-86°$ $-78°$	$+2.05$	-2.34	-2.6
Green	$-79°$ $-65°$	$+1.31$	-4.1	$+1.1$
Brown	$-86°$ $-78°$	$+2.35$	-1.16	$+0.2$
Pink	$-79°$ $-65°$	$+0.87$	-4.1	$+1.1$
Purple	$-86°$ $-78°$	$+2.05$	-1.16	$+0.2$

the case where $\mathcal{A}^N_{CP}$ is plotted with S_{LL}. Here we can see that the value of $\mathcal{A}^N_{CP}$ increases from -0.018 to 0.055 in $\mathcal{S}1$ and -0.035 to 0.035 in the second scenario, $\mathcal{S}2$. In scenario $\mathcal{S}3$, the maximum value of normal CP-violation asymmetry is 0.05, when we have $\tau^+\tau^-$ as the final-state leptons and the values of $\varphi_{sb} = 160°$ and $\lvert \mathcal{B}_{sb} \rvert = 5 \times 10^{-3}$. It is shown in Fig. 10 with the orange dot.

F. Transverse polarized *CP*-violation asymmetry

In the same fashion, the transverse polarized CP-violation asymmetry $\mathcal{A}^T_{CP}$ is also m_l suppressed, which is visible from $\mathcal{H}_6$ appearing in the function $\mathcal{Q}^T$. The graphs given in Figs. 11(a) and 12(a) just strengthen this argument, where $\mathcal{A}^T_{CP}$ is an order of magnitude suppressed in $B_s \to \varphi\mu^+\mu^-$ compared to $B_s \to \varphi\tau^+\tau^-$. From Figs. 11(b) and 12(b), it is clear that in case of the τ's as final state leptons, the value of the $\mathcal{A}^T_{CP}$ reaches 0.1 in a certain parametric space of the Z' scenario $\mathcal{S}1$.

By varying the Z' parameters in the range given in Eq. (50), the trend of transverse CP-violation asymmetry is shown by different colors of dots in Fig. 12. For $\varphi_{sb} = 160°$, $\lvert \mathcal{B}_{sb} \rvert = 5 \times 10^{-3}$ in scenario $\mathcal{S}3$, the value of transverse polarized CP-violation asymmetry in $B_s \to \varphi\tau^+\tau^-$ is close to its maximum value in $\mathcal{S}1$, and this is shown by the orange dot in Fig. 12(b). This can be measured in different collider experiments such as Belle II and LHCb.

V. CONCLUSION

In summary, we have analyzed the effects of NP coming through the neutral Z' boson on the polarized branching ratio, unpolarized and polarized CP-violation asymmetries in $B_s \to \varphi\ell^+\ell^-$ decays. We observed that the polarized branching ratio shows a clear signal of the Z' model, especially for the extreme values of the parameters corresponding to this model, and the values of $\mathcal{BR}_L$ and $\mathcal{BR}_T$ are almost 3 times the SM values for both μ and τ as final-state leptons. It is well known that in the SM, the CP-violation asymmetry is negligible, whereas in the present study we have seen that the unpolarized CP-violation asymmetry is considerable in both $B_s \to \varphi\mu^+\mu^-$ and $B_s \to \varphi\tau^+\tau^-$ channels, and hence it is giving a clear message of NP arising from the neutral Z' boson. In addition, all the polarized CP-violation asymmetries are significantly large in $B_s \to \varphi\tau^+\tau^-$ decay, and they show a strong dependence on the parameters of the Z' model. We keep in view that the detection of leptons' polarization effects is really a daunting task for experiments like ATLAS, CMS, and LHCb, but if we can just keep this issue aside, these CP-violation asymmetries which suffer less from hadronic uncertainties provide us a useful probe to establish the NP coming through the Z' model.

[1] F. Gursey and M. Serdaroglu, Lett. Nuovo Cimento **21**, 28 (1978).

[2] G. Buchalla, G. Burdman, C. T. Hill, and D. Kominis, Phys. Rev. D **53**, 5185 (1996).

[3] E. Nardi, Phys. Rev. D **48**, 1240 (1993).

[4] J. Bernabeu, E. Nardi, and D. Tommasini, Nucl. Phys. **B409**, 69 (1993).

[5] V. Barger, M. Berger, and R. J. Phillips, Phys. Rev. D **52**, 1663 (1995).

[6] E. Eichten, I. Hinchliffe, K. D. Lane, and C. Quigg, Rev. Mod. Phys. **56**, 579 (1984).

[7] P. Langacker and M. Plumacher, Phys. Rev. D **62**, 013006 (2000).

[8] J. L. Lopez and D. V. Nanopoulos, Phys. Rev. D **55**, 397 (1997).

[9] B. B. Sirvanli, Mod. Phys. Lett. A **23**, 347 (2008).

[10] A. Leike, Phys. Rep. **317**, 143 (1999).

[11] T. K. Kuo and N. Nakagawa, Phys. Rev. D **31**, 1161 (1985); Phys. Rev. D**32**, 306 (1985).

[12] K. K. Gan, Phys. Lett. B **209**, 95 (1988).

[13] E. Nardi, Phys. Rev. D **48**, 1240 (1993).

[14] B. Holdom, Phys. Lett. B **339**, 114 (1994).

[15] X. Zhang and B. L. Young, Phys. Rev. D **51**, 6584 (1995).

[16] B. Holdom and M. V. Ramana, Phys. Lett. B **365**, 309 (1996).

[17] S. Chaudhuri, S. W. Chung, G. Hockney, and J. Lykken, Nucl. Phys. **B456**, 89 (1995).

[18] G. Cleaver, M. Cvetic, J. R. Espinosa, L. Everett, and P. Langacker, Nucl. Phys. **B525**, 3 (1998).

[19] Y. Zhang and Z. Cai, arXiv:1106.0163.

[20] A. Kundu, Phys. Lett. B **370**, 135 (1996).

[21] J. Erler and P. Langacker, Phys. Rev. Lett. **84**, 212 (2000).

[22] C. Caso *et al.*, Eur. Phys. J. C **3**, 1 (1998).

[23] P. Langacker, Rev. Mod. Phys. **81**, 1199 (2009).

[24] M. S. Carena, A. Daleo, B. A. Dobrescu, and T. M. P. Tait, Phys. Rev. D **70**, 093009 (2004).

[25] M. Fattori, G. Roati, B. Deissler, C. D'Errico, M. Zaccanti, M. Jona-Lasinio, L. Santos, M. Inguscio, and G. Modugno, Phys. Rev. Lett. **101**, 190405 (2008).

[26] A. Abulencia *et al.* (CDF Collaboration), Phys. Rev. Lett. **96**, 211801 (2006).

[27] P. Langacker and M. Plumacher, Phys. Rev. D **62**, 013006 (2000).

[28] V. Barger, L. Everett, J. Jiang, P. Langacker, T. Liu, and C. Wagner, Phys. Rev. D **80**, 055008 (2009); J. High Energy Phys. 12 (**2009**) 048.

[29] Q. Chang, X.-Q. Li, and Y.-D. Yang, J. High Energy Phys. 02 (**2010**) 082.

[30] V. Barger, C.-W. Chiang, J. Jiang, and P. Langacker, Phys. Lett. B **596**, 229 (2004); K. Cheung, C.-W. Chiang, N. G. Deshpande, and J. Jiang, Phys. Lett. B **652**, 285 (2007); X.-G. He and G. Valencia, Phys. Rev. D **74**, 013011 (2006); S. Baek, J. H. Jeon, and C. S. Kim, Phys. Lett. B **664**, 84 (2008); S. Sahoo, C. K. Das, and L. Maharana, Int. J. Mod. Phys. A **26**, 3347 (2011).

[31] M. Bona *et al.* (UTfit Collaboration), PMC Phys. A **3**, 6 (2009); C.-H. Chen, Phys. Lett. B **683**, 160 (2010); N. G. Deshpande, X.-G. He, and G. Valencia, Phys. Rev. D **82**, 056013 (2010); J. E. Kim, M.-S. Seo, and S. Shin, Phys. Rev. D **83**, 036003 (2011); P. J. Fox, J. Liu, D.

Tucker-Smith, and N. Weiner, Phys. Rev. D **84**, 115006 (2011); Q. Chang, R.-M. Wang, Y.-G. Xu and X.-W. Cui, Chin. Phys. Lett. **28**, 081301 (2011).

[32] C. Bobeth and U. Haisch, Acta Phys. Pol. B **44**, 127 (2013).

[33] A. K. Alok, S. Baek, and D. London, J. High Energy Phys. 07 (**2011**) 111;

[34] V. Barger, C.-W. Chiang, P. Langacker, and H.-S. Lee, Phys. Lett. B **580**, 186 (2004); J. Hua, C. S. Kim, and Y. Li, Eur. Phys. J. C **69**, 139 (2010); Q. Chang, X.-Q. Li, and Y.-D. Yang, J. High Energy Phys. 04 (**2010**) 052; Q. Chang and Y.-H. Gao, Nucl. Phys. **B845**, 179 (2011); Y. Li, J. Hua, and K.-C. Yang, Eur. Phys. J. C **71**, 1775 (2011); C.-W. Chiang, Y.-F. Lin, and J. Tandean, J. High Energy Phys. 11 (**2011**) 083; S. Sahoo, C. K. Das, and L. Maharana, Int. J. Mod. Phys. A **24**, 6223 (2009); N. Katrici and T. M. Aliev, J. Phys. G **40**, 085005 (2013).

[35] V. Barger, C.-W. Chiang, P. Langacker, and H.-S. Lee, Phys. Lett. B **598**, 218 (2004); R. Mohanta and A. K. Giri, Phys. Rev. D **79**, 057902 (2009); Q. Chang, X.-Q. Li, and Y.-D. Yang, J. High Energy Phys. 05 (**2009**) 056; J. Hua, C. S. Kim, and Y. Li, Phys. Lett. B **690**, 508 (2010); Q. Chang, X.-Q. Li, and Y.-D. Yang, Int. J. Mod. Phys. A **26**, 1273 (2011); Q. Chang and Y.-D. Yang, Nucl. Phys. **B852**, 539 (2011); L. Hofer, D. Scherer, and L. Vernazza, J. High Energy Phys. 02 (**2011**) 080; Y. Li, X.-J. Fan, J. Hua, and E.-L. Wang, arXiv:1111.7153; S. Sahoo, C. K. Das, and L. Maharana, Phys. At. Nucl. **74**, 1032 (2011); S. Sahoo and L. Maharana, Indian J. Pure Appl. Phys. **46**, 306 (2008).

[36] I. Ahmed, Phys. Rev. D **86**, 095022 (2012).

[37] I. Ahmed, M. Jamil Aslam, and M. Ali Paracha, Phys. Rev. D **88**, 014019 (2013).

[38] G. Buchalla, A. J. Buras, and M. E. Lautenbacher, Rev. Mod. Phys. **68**, 1125 (1996).

[39] A. J. Buras and M. Munz, Phys. Rev. D **52**, 186 (1995).

[40] A. J. Buras, M. Misiak, M. Munz, and S. Pokorski, Nucl. Phys. **B424**, 374 (1994).

[41] F. Kruger and L. M. Sehgal, Phys. Lett. B **380**, 199 (1996).

[42] B. Grinstein, M. J. Savag, and M. B. Wise, Nucl. Phys. **B319**, 271 (1989).

[43] G. Cella, G. Ricciardi, and A. Vicere, Phys. Lett. B **258**, 212 (1991).

[44] C. Bobeth, M. Misiak, and J. Urban, Nucl. Phys. **B574**, 291 (2000).

[45] H. H. Asatrian, H. M. Asatrian, C. Grueb, and M. Walker, Phys. Lett. B **507**, 162 (2001).

[46] M. Misiak, Nucl. Phys. **B393**, 23 (1993); Nucl. Phys.**B439**, 461(E) (1995).

[47] T. Huber, T. Hurth, and E. Lunghi, arXiv:0807.1940.

[48] A. Ali, P. Ball, L. T. Handoko, and G. Hiller, Phys. Rev. D **61**, 074024 (2000).

[49] A. J. Buras and M. Munz, Phys. Rev. D **52**, 186 (1995).

[50] C. S. Lim, T. Morozumi, and A. I. Sanda, Phys. Lett. B **218**, 343 (1989).

[51] D. Melikhov, N. Nikitin, and S. Simula, Phys. Lett. B **430**, 332 (1998).

[52] J. M. Soares, Nucl. Phys. **B367**, 575 (1991).

[53] G. M. Asatrian and A. Ioannisian, Phys. Rev. D **54** (1996) 5642.

[54] C.-W. Chiang, R.-H. Li, and C.-D. Lu, Chin. Phys. C **36**, 14 (2012).

[55] Q. Chang, Nucl. Phys. **B845**, 179 (2011); Y. Li, J. Hua, and K.-C. Yang, Eur. Phys. J. C **71**, 1775 (2011).

[56] K. Cheung, C.-W. Chiang, N. G. Deshpande, and J. Jiang, Phys. Lett. B **652**, 285 (2007); C. H. Chen and H. Hatanaka, Phys. Rev. D **73**, 075003 (2006); C.-W. Chiang, N. G. Deshpande, and J. Jiang, J. High Energy Phys. 08 (**2006**) 075.

[57] V. Barger, C.-W. Chiang, P. Langacker, and H.-S. Lee, Phys. Lett. B **580**, 186 (2004); V. Barger, L. Everett, J. Jiang, P. Langacker, T. Liu, and C. Wagner, Phys. Rev. D **80**, 055008 (2009); R. Mohanta and A. K. Giri, Phys. Rev. D **79**, 057902 (2009); J. Hua, C. S. Kim, and Y. Li, Eur. Phys. J. C **69**, 139 (2010).

[58] P. Ball and V. M. Braun, Phys. Rev. D **58**, 094016 (1998).

[59] T. M. Aliev, A. Ozpineci, and M. Savc, Phys. Lett. B **511**, 49 (2001).

[60] K. S. Babu, K. R. S. Balaji, and I. Schienbein, Phys. Rev. D **68**, 014021 (2003).

[61] T. M. Aliev, V. Bashiry, and M. Savci, Eur. Phys. J. C **31**, 511 (2003); V. Bahiry, Phys. Rev. D **77**, 096005 (2008); V. Bashiry, N. Shrikhanghah, and K. Zeynali, Phys. Rev. D **80**, **015016** (2009).

[62] Q. Chang, X. Q. Li, and Y. D. Yang, J. High Energy Phys. 02 (**2010**) 082.

[63] M. Bona *et al.* (UTfit Collaboration), PMC Phys. A **3**, 6 (2009).

[64] V. Abazov, *et al.* (D0 Collaboration), D0 Conference Note No. 6098-CONF.

[65] T. Aaltonen, *et al.* (CDF Collaboration), Phys. Rev. D **85**, 072002 (2012).

[66] R. Aaij *et al.* (LHCb Collaboration), Phys. Rev. Lett. **108**, 101803 (2012); (LHCb Collaboration), Phys. Lett. B **707**, 497 (2012).

[67] V. Abazov *et al.* (CDF Collaboration), Phys. Rev. D **84**, 052007 (2011).

[68] X.-Q. Li, Y.-M. Li, G.-R. Lin, and F. Su, J. High Energy Phys. 05 (**2012**) 049.

[69] M. Iwasaki *et al.* (Belle Collaboration), Phys. Rev. D **72**, 092005 (2005).

[70] J. P. Lees *et al.* (*BABAR* Collaboration), arXiv:1204.3993.

[71] R. Aaij *et al.* (LHCb Collaboration), Phys. Rev. Lett. **108**, 181806 (2012).

[72] R. Aaij *et al.* (LHCb Collaboration), Phys. Rev. Lett. **108**, 231801 (2012).

[73] T. M. Aliev, K. Azizi, and M. Savci, Phys. Lett. B **718**, 566 (2012).